Quaternary Science Reviews 133 (2016) 28–47

Contents lists available at ScienceDirect

Quaternary Science Reviews

journal homepage: www.elsevier.com/locate/quascirev

# Holocene glacier variability and Neoglacial hydroclimate at Ålfotbreen, western Norway

Marthe Gjerde [a, c, *], Jostein Bakke [a], Kristian Vasskog [a, b], Atle Nesje [a, b], Anne Hormes [c, d]

[a] Department of Earth Science and Bjerknes Centre for Climate Research, University of Bergen, Allégaten 41, NO-5007, Bergen, Norway
[b] Uni Research Climate AS, Allégaten 55, NO-5007, Bergen, Norway
[c] Department of Arctic Geology, The University Centre in Svalbard, NO-9171, Longyearbyen, Norway
[d] Department of Earth Sciences, University of Gothenburg, SE-405 30, Gothenburg, Sweden

ARTICLE INFO

*Article history:*
Received 29 May 2015
Received in revised form
26 November 2015
Accepted 8 December 2015
Available online xxx

*Keywords:*
Glacier
Lake sediments
Holocene
Neoglacial
Winter precipitation
Hydroclimate
ELA
Western Norway
Ålfotbreen

ABSTRACT

Glaciers and small ice caps respond rapidly to climate perturbations (mainly winter precipitation, and summer temperature), and the mass-balance of glaciers located in western Norway is governed mainly by winter precipitation (Pw). Records of past Pw can offer important insight into long-term changes in atmospheric circulation, but few proxies are able to accurately capture winter climate variations in Scandinavia. Reconstructions of equilibrium-line-altitude (ELA) variations from glaciers that are sensitive to changes in Pw therefore provide a unique opportunity to quantify past winter climate in this region. Here we present a new, Holocene glacier activity reconstruction for the maritime ice cap Ålfotbreen in western Norway, based on investigations of distal glacier-fed lake sediments and modern mass balance measurements (1963–2010). Several lake sediment cores have been subject to a suite of laboratory analyses, including measurements of physical parameters such as dry bulk density (DBD) and loss-on-ignition (LOI), geochemistry (XRF), surface magnetic susceptibility (MS), and grain size distribution, to identify glacial sedimentation in the lake. Both radiocarbon (AMS $^{14}$C) and $^{210}$Pb dating were applied to establish age-depth relationships in the sediment cores. A novel approach was used to calibrate the sedimentary record against a simple ELA model, which allowed reconstruction of continuous ELA changes for Ålfotbreen during the Neoglacial (when Ålfotbreen was present, i.e. the last ~1400 years). Furthermore, the resulting ELA variations were combined with an independent summer temperature record to calculate Neoglacial Pw using the 'Liestøl equation'. The resulting Pw record is of higher resolution than previous reconstructions from glaciers in Norway and shows the potential of glacier records to provide high-resolution data reflecting past variations in hydroclimate. Complete deglaciation of the Ålfotbreen occurred ~9700 cal yr BP, and the ice cap was subsequently absent or very small until a short-lived glacier event is seen in the lake sediments ~8200 cal yr BP. The ice cap was most likely completely melted until a new glacier event occurred around ~5300 cal yr BP, coeval with the onset of the Neoglacial at several other glaciers in southwestern Norway. Ålfotbreen was thereafter absent (or very small) until the onset of the Neoglacial period ~1400 cal yr BP. The 'Little Ice Age' (LIA) ~650–50 cal yr BP was the largest glacier advance of Ålfotbreen since deglaciation, with a maximum extent at ~400–200 cal yr BP, when the ELA was lowered approximately 200 m relative to today. The late onset of the Neoglacial at Ålfotbreen is suggested to be a result of its low altitude relative to the regional ELA. A synthesis of Neoglacial ELA fluctuations along the coast of Norway indicates a time-transgressive trend in the maximum extent of the LIA, which apparently seems to have occurred progressively later as we move northwards. We suggest that this trend is likely due to regional winter precipitation differences along the coast of Norway.



## 1. Introduction

In order to create robust projections of future climate change, it is of great importance to understand past natural climate variability, as this may help to discern the relative importance of

* Corresponding author. Department of Earth Science, University of Bergen, Allégaten 41, NO-5007, Bergen, Norway.
*E-mail addresses:* Marthe.gjerde@uib.no (M. Gjerde), Jostein.bakke@uib.no (J. Bakke), Kristian.vasskog@uib.no (K. Vasskog), Atle.nesje@uib.no (A. Nesje), Anne.hormes@gvc.gu.se (A. Hormes).

http://dx.doi.org/10.1016/j.quascirev.2015.12.004

natural and anthropogenic forcing on the climate system (Masson-Delmotte et al., 2013). Glaciers and ice caps are excellent climate indicators, as they respond to changes in temperature and precipitation; and thus, records of past glacier fluctuations can give information about past climate variability (Oerlemans, 2005). Presently, the annual mass-balance of small plateau glaciers located at the coast of south-western Norway is controlled mainly by winter accumulation, and mass-balance measurements from this area are therefore useful tools for exploring past variations in winter precipitation (Marzeion and Nesje, 2012). Glacier mass-balance data are, however, generally scarce; in some cases discontinuous; and extend only a few decades back in time. In order to expand records of glacier variability and associated winter precipitation beyond the instrumental record we therefore utilize natural archives, such as continuous sedimentary records from distal glacier-fed lakes.

Distal glacier-fed lakes act as traps for glacially eroded sediments that are transported by glacial meltwater streams downvalley, and by quantifying the influx of glacial sediment to these lakes it is possible to reconstruct continuous changes in upstream glacial erosion and hence glacier size through time. A large number of distal glacier-fed lakes have been investigated throughout Scandinavia, together providing an extensive overview of past glacier variability in this region (Karlén, 1976, 1981; Nesje et al., 1991; Dahl and Nesje, 1992; Karlén and Matthews, 1992; Dahl and Nesje, 1994; Matthews et al., 2000; Nesje et al., 2000b, 2001; Lie et al., 2004; Rosqvist et al., 2004; Bakke et al., 2005; Shakesby et al., 2007; Bakke et al., 2010; Vasskog et al., 2012; Bakke et al., 2013; Røthe et al., 2015; Wittmeier et al., 2015).

Some of these records present only relative changes in glacial input to the lakes, but in cases where dated moraine ridges are available to reconstruct the glacier extent at specific points in time, lake records can be calibrated to produce continuous reconstructions of changes in equilibrium-line altitude (ELA) (e.g. Nesje et al., 2001; Dahl et al., 2003; Bakke et al., 2010; Røthe et al., 2015). If an independent record of summer temperature is available, estimates of past winter precipitation can be extracted from continuous ELA reconstructions (e.g. Dahl and Nesje, 1996; Bjune et al., 2005) through the so-called 'Liestøl equation' described by O. Liestøl in Sissons (1979); a mathematical expression based on the empirical relationship between annual precipitation and summer temperature at the ELA of ten Norwegian glaciers.

Ålfotbreen is the westernmost ice cap in Norway, and the extreme maritime nature of this plateau glacier makes it a particularly interesting target for high-resolution reconstructions of past glacier fluctuations. From CE1963-2010, changes in the annual mass balance of Ålfotbreen have been mainly governed by the amount of winter accumulation ($R^2 = 0.71$) (data from: Kjøllmoen, 2011), but the relative importance of winter accumulation vs. summer ablation might be different when longer timescales are considered (Trachsel and Nesje, 2015). Long-term ELA reconstructions are therefore valuable tools for evaluating long-term natural variability of past winter climate. Here we present (1) a relative glacier fluctuation reconstruction of the Ålfotbreen ice cap during the Holocene; (2) a high-resolution reconstruction of Neoglacial ELA variations; (3) a constraint on the timing of the 'Little Ice Age' (LIA) maximum; and (4) reconstructed Neoglacial winter precipitation for the study area. Finally, we discuss the climatic implications of our findings in relation to other palaeoclimatic records in the North Atlantic region, including glacier records and winter precipitation reconstructions from other parts of Scandinavia, as well as possible forcing mechanisms that could explain the observed glacier variability.

## 2. Study area

### 2.1. Glacier, climate and bedrock

The Ålfotbreen plateau glacier (here defined as encompassing the two separate ice caps 'Ålfotbreen' and 'Blåbreen' with surrounding ice patches) covers an area of 15.5 km$^2$ (Andreassen et al., 2012), where the majority of the glaciated area is constrained to a limited altitude interval near the maximum elevation (Kjøllmoen, 2011; Andreassen et al., 2012). The glacier covers ~2.5 km$^2$ (~6%) of the total catchment area (41.5 km$^2$) of the downstream glacier-fed lake Grøndalsvatnet (see Section 2.2 below). Ålfotbreen ('Å' in Fig. 1C) and Blåbreen ('B' in Fig. 1C) are separated by a steep cliff in the area's tilted sedimentary Devonian bedrock (Bryhni and Lutro, 2000). Because of the distinct steps in the landscape, along with the narrow hypsometry of Ålfotbreen (altitude range <600 m), the ice cap does not feature very prominent outlet glaciers. Two adjacent north-facing outlet glaciers named Ålfotbreen (4.0 km$^2$; not to be confused with the ice cap itself) and Hansebreen (2.8 km$^2$) have been subject to mass-balance studies since CE1963 and CE1986, respectively (Kjøllmoen, 2011). During recent years the annual ELA has been raised above the highest elevation of the ice cap (>1382 m a.s.l.) several times (Kjøllmoen, 2011). See Fig. 1 for an overview of the study area, and Fig. 2 for an overview of the narrow hypsometry of the two outlet glaciers mentioned above. From here on, the term 'Ålfotbreen' includes both outlet glaciers mentioned above, the two ice caps Blåbreen and Ålfotbreen as well as the surrounding ice patches, unless stated otherwise.

Relative to area, Ålfotbreen has the largest annual mass turnover of the monitored glaciers in Norway, with the highest recorded values for both winter accumulation and summer ablation (Kjøllmoen, 2011). For Ålfotbreen, winter accumulation is considered more important in determining its net mass balance than summer ablation (Nesje, 2005), and a large gain in mass between CE1989-95 was mainly caused by high winter balance (Andreassen et al., 2005). Despite the large mass turnover, Ålfotbreen is ranked as the most vulnerable glacier in Norway, mainly due to its narrow hypsometric distribution above the steady-state ELA (~200 m, Fig. 2), and it might therefore be one of the first glaciers to disappear completely in a warmer future climate (Nesje et al., 2008; Andreassen et al., 2012). Inferences about past extent and fluctuations of Ålfotbreen have previously been published by Nesje et al. (1995) and Sønstegaard et al. (1999); however, neither of these studies obtained a complete Holocene glacial history. Nesje et al. (1995) focused on the late-Holocene glacier history and avalanche activity, whereas Sønstegaard et al. (1999) were targeting the deglaciation history of the area. As an isolated ice cap from the main Scandinavian ice sheet during the Younger Dryas (YD), Ålfotbreen obtained its maximum YD extent just before the deposition of the Vedde Ash Bed (Sønstegaard et al., 1999). The further history of deglaciation and Holocene glacier variations has so far been poorly constrained for Ålfotbreen (Nesje, 2009).

The present climate of the study area is maritime with a mean CE1961-1990 summer temperature (Ts; 1 May-30 September) of 12.12 °C (climate station 58070 Sandane, ca. 30 km east of Ålfotbreen; 51 m a.s.l.). Mean CE1961-1990 winter precipitation (Pw; 1 October – 30 April) at the 57680 Eikefjord climate station (ca. 20 km south-southwest of Ålfotbreen; 30 m a.s.l.) is 1677 mm (eKlima.no); and snow accumulations of up to 8–10 m during winter are not unusual at the top of Ålfotbreen (Andreassen et al., 2012).

### 2.2. Catchment lakes and geomorphological setting

Lake Grøndalsvatnet (~0.27 km$^2$; N 61°41′, E05°34′) is located

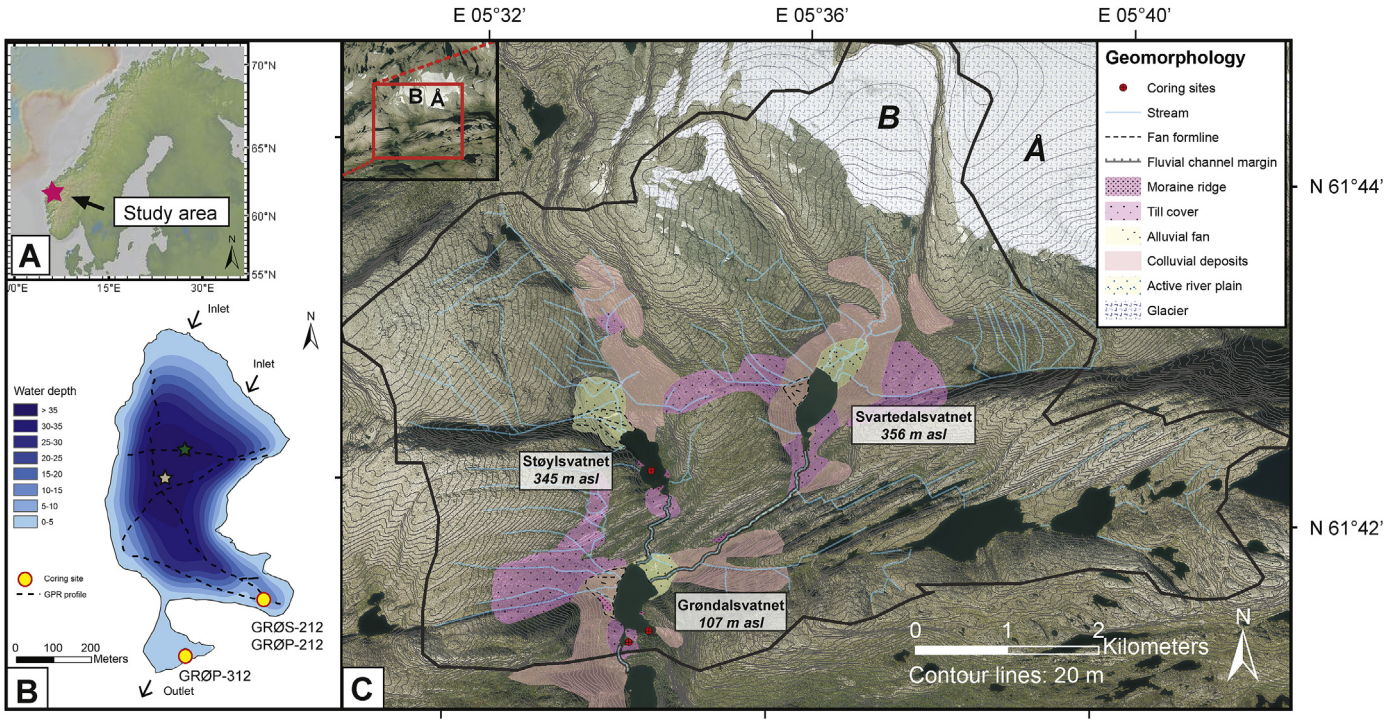


**Fig. 1.** Overview of the study area. A) Study site location in Scandinavia; B) Bathymetrical map of Grøndalsvatnet, showing coring sites and GPR profiles (water depth in m). Green asterisk marks coring location from Nesje et al. (1995). Grey asterisk marks coring location for GRØP-112 (not analysed, see Section 4.1); C) Geomorphological map of the catchment area with coring sites marked in red; black solid line outlines the catchment limit. Upper left shows the area surrounding the ice cap. (For interpretation of the references to colour in this figure legend, the reader is referred to the web version of this article.)

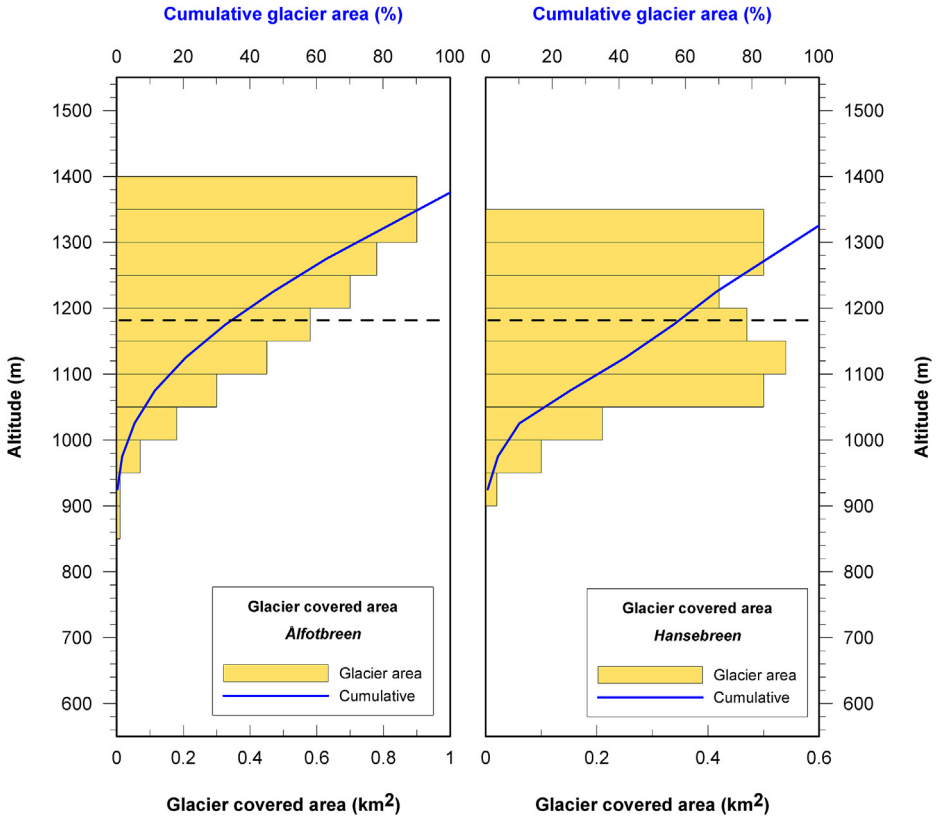


**Fig. 2.** Hypsometry of two outlet glaciers from Ålfotbreen ice cap: Ålfotbreen and Hansebreen. Stippled line represents calculated steady-state ELA (~1180 m.a.s.l.) for Ålfotbreen (for the monitoring period CE1963-2010).

south of Ålfotbreen, at an elevation of 107 m a.s.l. Deep glacial troughs and steep cliffs characterize the surrounding catchment topography. The catchment is dominated by exposed bedrock, with unconsolidated sedimentary deposits being limited mainly to the large inlet delta in the northern end of the lake, a distinct colluvial fan along its western shore, and a moraine ridge close to the outlet (Fig. 1). Vegetation cover is relatively dense across most of the colluvial fan, the moraine ridge, and the remaining till cover, up to an altitude of about 500–600 m a.s.l., whereas the inlet delta is covered by farmland. The main inlet is a river transporting meltwater from Ålfotbreen into the lake across the delta, although the meltwater needs to pass through the upstream lake Svartedalsvatnet (356 m a.s.l.) before reaching Grøndalsvatnet. This setting allows only relatively fine-grained glacial sediments to continue downstream to Grøndalsvatnet. Lake Støylsvatnet (~0.18 $km^2$; N 61°42′, E05°34′) is also situated upstream from Grøndalsvatnet at an elevation of 345 m a.s.l., but this lake is part of a different catchment area and the lake is not fed by glacial meltwater from Ålfotbreen at present. A small river presently drains from Støylsvatnet into Grøndalsvatnet across the western end of the inlet delta. Apart from this, only three smaller creeks drain into the lake, all of which are orders of magnitude smaller than the main inlet. Støylsvatnet has probably received glacial meltwater from Ålfotbreen in the past when the ice cap covered a larger area, and Støylsvatnet was therefore targeted as a potential 'threshold lake' (e.g. Dahl et al., 2003; Briner et al., 2010) to constrain the timing of particularly large glacier advances; e.g. during the 'Little Ice Age' (LIA). A soft sediment map for Grøndalsvatnet is shown in Supplementary Fig. S1, and a bathymetrical map of Støylsvatnet in Supplementary Fig. S2.

## 3. Methods

A combination of geomorphological field mapping, studies of aerial photographs and available online data on superficial deposits from the Geological Survey of Norway (ngu.no) and the Norwegian Mapping Authority (norgeskart.no) form the basis for the data presented in the geomorphological map of the area (Fig. 1). The reconstruction of Holocene glacier fluctuations at Ålfotbreen is based on a range of different laboratory analyses (see below) performed on the sediment cores obtained from the distal glacier-fed lake Grøndalsvatnet and the 'threshold lake' Støylsvatnet. The term 'threshold lake' is adapted from Briner et al. (2010) as a lake where the catchment area has been partly covered by advancing ice during certain periods, so that the non-glacial lake undergoes a transformation to a glacier-fed lake (without the lake basin being overridden by ice). As a result, the lake sediment fill consist of organic-rich sediments during periods where ice extent is relatively small (e.g. before the LIA), and minerogenic-rich sediments during periods of relatively large ice extent (e.g. during the LIA) (Briner et al., 2010). A robust chronology has been established for the cores through AMS radiocarbon ($^{14}C$) dating of terrestrial macrofossils in combination with lead ($^{210}Pb$) ages obtained on the most recent sediments.

### 3.1. Geophysical survey and lake sediment coring

Prior to lake coring, combined echo sounding and ground penetrating radar (GPR) surveys of Lake Grøndalsvatnet were conducted in May 2012 to determine suitable coring sites. GPR profiles were collected using a RAMAC GPR from Malå with a 25 MHz RTA antenna in order to map the soft sediment thickness, whereas the bathymetry was measured with an echo sounder (Fig. 1 and S1). Three cores; GRØP-112 (239 cm); GRØP-212 (243 cm); and GRØP-312 (212.5 cm), were retrieved from a raft using a modified piston corer with a 110 mm diameter core tube (Nesje, 1992). The uppermost ~10 cm of GRØP-312 were lost during coring. In order to recover the sediment-water interface, two short HTH (Renberg-type) gravity cores, GRØS-112 and GRØS-212, were collected adjacent to the GRØP-112 and GRØP-212 coring sites, respectively. In order to avoid disturbances from colluvial activity, mass-movement on the delta front, and any possible long-term effects of delta progradation, the main cores (GRØP-212/GRØS-212) were retrieved in a backwater area close to the lake outlet (Fig. 1).

In June 2014, the threshold lake Støylsvatnet was cored to investigate recent glacier fluctuations in the area using $^{210}Pb$ dates for age estimation. Prior to coring, an echo sounder combined with the 'Dr Depth' software was used to record the bathymetry of the lake (Fig. S2). Two short cores; STØS-114 (30 cm) and STØS-214 (32 cm), were both collected using a UWITEC gravity coring device.

### 3.2. Laboratory analyses

The sediment cores were split lengthwise in the laboratory and one half of each core was stored for reference. Core surfaces were then carefully cleaned and photographed. Lithofacies and sedimentological structures and textures were described in detail before scanning and sub-sampling was initiated.

Geochemical data and radiographic images were obtained using an ITRAX x-ray fluorescence (XRF) Scanner (Croudace et al., 2006) in EARTHLAB, Department of Earth Science, University of Bergen. A molybdenum (Mo) x-ray tube was used for radiographic measurements, whereas XRF analyses were performed applying a chromium (Cr) tube, with a down-core resolution of 500 μm. Power settings of 30 kV and 35 mA were used with a 10 s counting time. Down-core variations in surface magnetic susceptibility (MS) were measured on the split cores at 0.2 cm resolution using a Bartington MS2E point sensor.

Standard procedures for estimating weight loss-on-ignition (LOI, %), dry bulk density (DBD, $g/cm^3$) and water content (WC, %) were followed (Dean, 1974; Heiri et al., 2001), and the cores were sampled for this purpose every 0.5 cm (GRØP-212; $n = 486$, GRØP-312; $n = 425$, GRØS-212; $n = 59$, STØS-214; $n = 64$) using a syringe for fixed volume extraction (1 $cm^3$). The samples were weighed and dried overnight at 105 °C before being weighed again for DBD and WC. Following subsequent ignition at 550 °C for one hour, the samples were cooled in a desiccator and reweighed for LOI.

Samples from minerogenic sections of GRØP-212 ($n = 38$) were analysed for grain-size distribution. 6–8 g samples (wet weight) were extracted and stirred for two days in a 5% $H_2O_2$ aqueous solution in order to remove possible organic bindings between grains. The samples were then stirred in a 0.05% Calgon (sodium hexametaphosphate) solution overnight. Finally, the material <63 μm was analysed using a Micromeritics Sedigraph 5100 and Mastertech 5.1 auto sampler. Each sample was analysed several times (five or six) and all of the runs were averaged in order to obtain the final grain-size distribution. The grain-size data were processed using the Gradistat v.8.0 software (Blott and Pye, 2001).

### 3.3. Chronology

A total of $n = 20$ samples of wet sediments with an average weight of 8 g were extracted every cm from the top 20 cm of GRØS-212. The samples were freeze-dried and submitted for $^{210}Pb$ dating (as well as measuring of $^{226}Ra$, $^{137}Cs$ and $^{241}Am$ by direct gamma assay) at the Environmental Radioactivity Research Centre, University of Liverpool. The same procedure of freeze-drying was

followed for the upper 12 cm of STØS-214, but here the sampling was done every 0.5 cm ($n = 24$). $^{210}$Pb ages obtained for GRØS-212 and STØS-214 are shown in Supplementary Tables S1 and S2, respectively.

A total of $n = 20$ terrestrial macrofossil samples (e.g. leaves, twigs, fruits, and seeds) were extracted from GRØP-212 and GRØP-312 and submitted for accelerator mass spectrometry (AMS) radiocarbon dating at the Poznan Radiocarbon Laboratory in Poland (Table 1). 1-cm sediment slices were extracted at selected depths and wet-sieved, after which plant macrofossils were handpicked and identified using a stereo microscope. Macrofossils were dried overnight at 50 °C and placed in sterilized glass vials before submission to AMS dating. At the radiocarbon laboratory, macrofossils were chemically prepared with acid-alkali-acid in a three-step treatment (http://www.radiocarbon.pl/).

Age-depth models were constructed using the 'clam' source code from Blaauw (2010), applied in the open-source statistical software 'R' (R Development Core Team, 2012). Radiocarbon ages are reported in calibrated radiocarbon years before present (cal yr BP; BP = 1950) and Common Era (CE). Several samples contained less than 1 mg of carbon (Poz-54061; Poz-54062; Poz-54066; Poz-54068; Poz-54070; Poz-54074; see Table 1) and a number of these were not included for modelling of the age-depth relationship (see Section 4.4).

### 3.4. Principal Component Analysis

The multivariate sedimentary data sets from GRØP-212 and GRØP-312 were explored using Principal Component Analysis (PCA) in order to detect patterns of shared variability between the measured proxies (e.g. Syms, 2008). Because PCA assumes linearity between the analysed variables (e.g. Bakke et al., 2013), the relationship between all variables in the dataset were examined individually using biplots and regression analysis to see whether any data transformation was needed before running the PCA. A logarithmic relationship was found between LOI and the other data, and LOI was therefore Log-transformed before analysis. The entire dataset was then standardized before running the PCA in the software Canoco for Windows (v. 4.5) (Lepš and Šmilauer, 2003).

In total, 11 variables were included in the PCA from both cores GRØP-212 and GRØP-312. In addition to the physical proxies DBD, LogLOI, and MS, geochemical elements that are commonly sensitive to changes in detrital input (Si, Ti, K, and Ca; e.g. Bakke et al. (2010)), redox processes (Fe and Mn; e.g. Naeher et al. (2013)), and grain-size (Rb and Sr; e.g. Vasskog et al. (2012)) were added into the analysis.

### 3.5. Instrumental meteorological data and mass-balance modelling

In order to reconstruct continuous ELA changes from distal glacier-fed lake sediments, the sediment parameters need to be calibrated against periods when the ELA is known or can be inferred. This calibration is commonly obtained using moraine ridges of known age (Dahl et al., 2003; Bakke et al., 2010), but this approach cannot be applied here as there are no observed distinct late-Holocene/LIA moraine ridges around Ålfotbreen. However, ELA measurements are available for Ålfotbreen (the outlet glacier) between CE1963 and CE2010 (Kjøllmoen, 2011), and this record can be extended by modelling the ELA using instrumental meteorological data. Nordli et al. (2005) applied a stepwise multiple regression and found that a combination of two atmospheric indices; the wintertime westerly geostrophic wind component (*uw*) and the summertime southerly shear vorticity ($\xi_v$s), was able to predict the ELA at Ålfotbreen with relatively high precision (Pearson's correlation coefficient, $r = 0.72$). These indices can be calculated from mean sea-level pressure (MSLP) data that are available back to CE1781 for northern Europe (Jones et al., 1999). However, some of the summertime MSLP data used in calculation of the shear vorticity index are not considered to be robust beyond CE1850 (Jones et al., 1999), and this index does not seem to capture long-term trends in summer temperature very well. However, over decadal timescales, summer temperatures along the west coast of Norway are strongly correlated with North Atlantic sea surface temperatures ($r = 0.88$) (Supplementary Fig. S3), and we therefore tested a reconstruction of the Atlantic Multidecadal Oscillation (AMO) (Mann et al., 2009) as an alternative predictor of summer ablation in our ELA model, and this resulted in a better fit ($r = 0.77$, $R^2 = 0.59$) with measured ELA than the model from Nordli et al. (2005). Thus, the ELA model employed here uses wintertime geostrophic wind (*uw*) (Nordli et al., 2005) and AMO temperature anomalies (Mann et al., 2009) as predictors, and is expressed as:

**Table 1**
Radiocarbon dates obtained for GRØP-212 and GRØP-312. Calibrated ages obtained using 'clam' (Blaauw, 2010). Samples marked* were rejected for the age-depth modelling in 'clam'.

| Core | Lab.no | Depth (cm) | Material | $^{14}$C age | ±2 sigma (cal yr BP) | $\delta^{13}$C (‰) | Remark |
|---|---|---|---|---|---|---|---|
| GRØP-212 | Poz-54060 | 10–11 | Terrestrial plant remains | 90 ± 35 BP | 15-268* | −26.6 | |
| GRØP-212 | Poz-54061 | 13–14 | Terrestrial plant remains | 105 ± 30 BP | 14-268* | −29.2 | TOC, 0.7mgC |
| GRØP-212 | Poz-54062 | 25–26 | Terrestrial plant remains | 115.12 ± 0.42 pMC | (-43)-8* | −32.4 | TOC, 0.4mgC |
| GRØP-212 | Poz-54063 | 30–31 | Terrestrial plant remains | 540 ± 30 BP | 514–633 | −28.1 | |
| GRØP-212 | Poz-54064 | 45–46 | Terrestrial plant remains | 1840 ± 30 BP | 1709–1864* | −23.6 | |
| GRØP-212 | Poz-54066 | 50–51 | Terrestrial plant remains | 1580 ± 40 BP | 1389–1551 | −32.7 | 0.3mgC |
| GRØP-212 | Poz-54067 | 80–81 | Terrestrial plant remains | 2540 ± 40 BP | 2491–2751 | −25.3 | |
| GRØP-212 | Poz-54068 | 110–111 | Terrestrial plant remains | 2600 ± 40 BP | 2512-2786* | −33.2 | TOC, 0.4mgC |
| GRØP-212 | Poz-61506 | 114–115 | Terrestrial plant remains | 3925 ± 35 BP | 4245–4498 | −25.8 | |
| GRØP-212 | Poz-54070 | 132–133 | Terrestrial plant remains | >0 BP | | | Too small |
| GRØP-212 | Poz-54071 | 150–151 | Terrestrial plant remains | 5910 ± 40 BP | 6654–6845 | −24.7 | |
| GRØP-212 | Poz-61505 | 180–181 | Terrestrial plant remains | 7740 ± 40 BP | 8433–8590 | −28.7 | |
| GRØP-212 | Poz-54072 | 185–186 | Terrestrial plant remains | 8030 ± 50 BP | 8663–9030* | −30.2 | |
| GRØP-212 | Poz-54073 | 230–231 | Terrestrial plant remains | 8720 ± 50 BP | 9550–9887 | −29.8 | |
| GRØP-312 | Poz-54074 | 10–11 | Terrestrial plant remains | 55 ± 35 BP | (-5)-259* | −28.3 | 0.8mgC |
| GRØP-312 | Poz-54075 | 30–31 | Terrestrial plant remains | 345 ± 30 BP | 314–483 | −24.3 | |
| GRØP-312 | Poz-54076 | 35–36 | Terrestrial plant remains | 460 ± 30 BP | 485–537 | −26.2 | |
| GRØP-312 | Poz-54077 | 47–48 | Terrestrial plant remains | 845 ± 35 BP | 686–899 | −25.4 | |
| GRØP-312 | Poz-54078 | 88–89 | Terrestrial plant remains | 1570 ± 30 BP | 1397–1533 | −29.9 | |
| GRØP-312 | Poz-54080 | 156–157 | Terrestrial plant remains | 2295 ± 30 BP | 2183–2354 | −24.8 | |

$$\mathrm{ELA} = (-29{*}uw) + (226{*}\mathrm{AMO}) + 1360(\text{m a.s.l.}) \quad \left(R^2 = 0.59,\ p < 0.003\right) \tag{1}$$

### 3.6. Quantifying winter precipitation

We use the approach presented by Dahl and Nesje (1996) for reconstructing winter precipitation (Pw), which is based on the close empirical relationship between mean ablation-season (1 May to 30 September) temperature (Ts) and Pw at the ELA of Norwegian glaciers; i.e. the 'Liestøl equation' (Sissons, 1979; Sutherland, 1984; Ballantyne, 1989). This relationship is expressed by the regression equation:

$$\mathrm{Pw} = 0.915\ e^{0.339\mathrm{Ts}} \quad \left(R^2 = 0.989,\ p < 0.0001\right) \tag{2}$$

where Pw is meters of water equivalents and Ts is the mean ablation season (summer) temperature at the ELA in °C. This implies that if the mean summer temperature at the ELA is measured/reconstructed, the mean winter precipitation can be calculated. Using an environmental lapse rate of 0.65 °C/100 m as in Sutherland (1984) and Oerlemans (1992), this gives a mean summer temperature (Ts) of 4.77 °C at the present steady-state ELA of Ålfotbreen at 1182 m a.s.l. (obtained through linear regression of net mass balance against measured ELAs for the period CE1963-2010, c.f. Fig. 2). Using Eq. (2), we find that the Pw required to balance summer ablation at the steady-state ELA is ~4.61 m. This procedure can be used to reconstruct past Pw at the ELA by combining a continuous ELA reconstruction with an independent temperature record (e.g. Dahl and Nesje, 1996; Bjune et al., 2005). Finally, winter precipitation can be calculated for a fixed altitude (e.g. sea level) by accounting for fluctuations in the ELA using the observed exponential increase in Pw with altitude of 8%/100 m in southern Norway (Haakensen, 1989).

## 4. Results

### 4.1. Lithostratigraphy

Core GRØP-112 (N61.68948 E5.56832; water depth: 39 m) was retrieved from the middle part of the Grøndalsvatnet basin, corresponding to the approximate location of the core studied by Nesje et al. (1995) (Fig. 1). Like Nesje et al. we found that the lacustrine stratigraphy at this site is dominated by rapidly deposited layers (e.g. avalanche-, flood- or debris-flow deposits); most likely introduced to the basin from a large alluvial fan west of the lake; and the core was therefore not considered for further analyses. Cores GRØP-212 (N61.68665 E5.57280; water depth: 12 m) and GRØP-312 (N61.68543 E5.56881; water depth: 5 m) were collected from the south-eastern parts of the lake, where the risk of disturbances from floods and colluvial events was considered to be lower and the distance to the main inlet is larger. The description of lithostratigraphy (below) refers to GRØP-212, because a hiatus in GRØP-312 indicates that this core is missing a large part of the lower sediments (i.e. lithostratigraphic units B; C; D; and parts of unit E; see below). The lithostratigraphic division of the core into nine units, A-I, is based on visual logging. A correlation was made between all cores based on XRF Ti count rates (Fig. 3), as this parameter distinguishes well the different sedimentary units.

Unit A (*206–243 cm*) consists of grey clayey- and silty-, highly-minerogenic sediments. The unit is massive and comprises varying grain sizes ranging from clay to fine sand. Thin (<0.5 cm) horizons with visible plant remains are relatively frequent, and a prominent horizon was sampled for radiocarbon dating (Poz-54073). DBD values are generally very high; decreasing upwards in the unit from 1.47 to 0.47 g/cm$^3$ and averaging at 0.98 g/cm$^3$. The opposite trend is observed for LOI, which increases from values around 5% in the lower part up to more than 9% in the topmost part of unit A, reflecting an increase in organic content.

Unit B (*187–206 cm*) consists of very dark greyish brown silty gyttja with lighter-coloured laminations that gradually becomes weaker upwards. DBD is relatively stable (around 0.5 g/cm$^3$), whereas LOI shows greater variability and an increasing trend (from ~7 to ~12%). An erosional contact marks the transition to unit C.

Unit C (*178–187 cm*) consists of greyish brown, chaotic, clayey- and silty minerogenic sediments in the lower part, and contains angular clasts up to ~0.5 cm diameter. The lower section of the unit (181–187 cm) is massive and can be distinguished both visually and in X-ray images (cf. Fig. 4). From 180 to 181 cm the sediments consist of laminated greyish-brown, silty gyttja, and from 178 to 180 cm it is characterized by a very dark brown, highly organic horizon rich in terrestrial plant remains. Unit C has a distinct development from highly minerogenic in the lower part (DBD = ~1.0 g/cm$^3$; LOI = ~4%) to highly organic in the upper part (DBD = ~0.4 g/cm$^3$; LOI = ~22%). The lower section of the unit (181–187 cm) is interpreted to have been deposited rapidly. The erosional contact at the base, the stirred appearance of the sediments, and the angular morphology of the grains suggest that this may be an avalanche deposit. The upper section of the unit, 178–180 cm, is interpreted to represent a flood event delivering organic detritus from the catchment area to the lake.

Unit D (*172–178 cm*) consists of very dark, greyish-brown silty gyttja with lighter-coloured laminations. The unit is characterised by a peak in all parameters except LOI, which decreases to a minimum of ~8% in this unit. X-ray images show that the sediments are relatively dense, which is also reflected in relatively high DBD values (~0.5–0.7 g/cm$^3$). The percentage of fine silt shows a distinct peak, rising from ~20 to 40% before decreasing again towards the top of the unit.

Unit E (*40.5–172 cm*) consists of very dark brown to olive brown gyttja with lighter-coloured laminations. The section from 120 to 130 cm has a lighter colour with more frequent laminations, and X-ray imagery shows that the sediments in that section are relatively dense compared to the sediments above and below. DBD values remain low and stable throughout the unit; with values averaging ~0.4 g/cm$^3$. LOI shows greater variability than DBD throughout unit E, fluctuating between ~12 and 21%, with the trend gently increasing. A dark brown horizon consisting mainly of plant remains is observed from 43.5 to 46 cm depth, and this section is interpreted to represent a flood event.

Unit F (*27–40.5 cm*) consists of dark, greyish-brown silty gyttja, and is largely a transitional unit from organic sediments at the base to more minerogenic sediments in the top. DBD increases from ~0.4 to a maximum of ~0.6 g/cm$^3$ through the unit, reflecting an increasing density that can also be seen in the radiographic images, while LOI decreases from ~13 to ~6%. Lighter-coloured laminations also increase in frequency upwards.

Unit G (*22–27 cm*) consists of olive brown silty gyttja that is slightly more organic than the underlying unit. DBD drops to an average of ~0.5 g/cm$^3$ and LOI increases to an average of ~9%.

Unit H (*6–22 cm*) consists of greyish brown, slightly organic, clayey silt. Several distinct peaks in DBD of up to ~1.0 g/cm$^3$ can be seen, and together with a colour change of the sediment this indicates a shift in the depositional environment. LOI shows an opposite pattern of DBD, with values averaging at 5%. A dark,

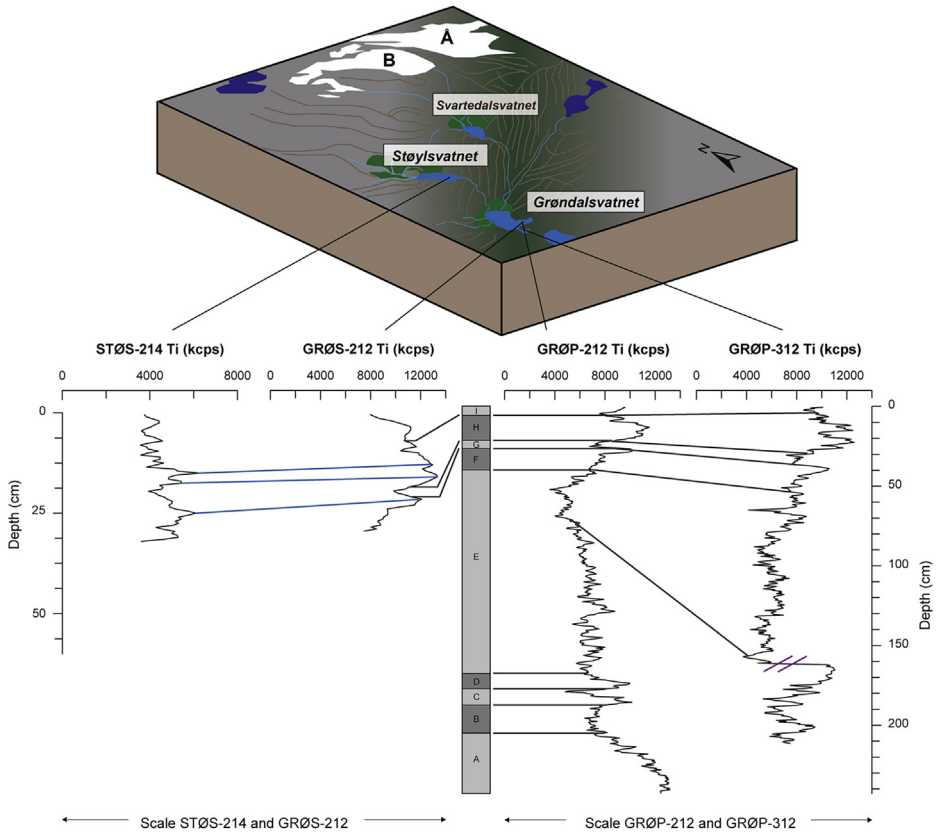


**Fig. 3.** Schematic 3D profile of the catchment area for Støylsvatnet and Grøndalsvatnet with visual correlation of the cores based on XRF Ti count rates (kcps) in combination with $^{210}$Pb and $^{14}$C ages and visual structures. Blue lines mark the correlation between Ti peaks in STØS-214 and GRØS-212. Note hiatus in GRØP-312 marked in purple (158 cm depth). (For interpretation of the references to colour in this figure legend, the reader is referred to the web version of this article.)

organic-rich horizon with LOI up to ~9% is seen from 8 to 10.5 cm, which consists predominantly of plant remains. This is interpreted to represent a layer of instantaneous deposition, most likely a flood event.

Unit I (*0–6 cm*) consists of very dark, greyish-brown silty gyttja. DBD lowers to an average value of ~0.5 g/cm$^3$, and LOI increases to ~7% on average.

In previous studies (e.g. Nesje et al., 2007; Vasskog et al., 2011), river flood deposits have been characterised by their brown colour, high-organic content, and large amount of terrestrial plant macrofossils, whereas horizons containing clasts >1 mm are interpreted as snow-avalanche deposits. Based on these criteria, the specific horizons ≥1 cm that have been interpreted as layers representing flood events and avalanche deposits (i.e. 'instantaneous' deposition, see Fig. 4) were omitted from the age-depth relationship modelling and further discussion of the results.

### 4.2. Magnetic susceptibility

In general, MS values in GRØP-212, GRØP-312, GRØS-212 and STØS-214 are quite low; on average 9; 8; 13 and 3 (Si $10^{-5}$), respectively. Because the bedrock in the catchment area consists of sandstones and conglomerates it contains a large proportion of the diamagnetic mineral quartz ($SiO_2$), which will return a net negative magnetic moment when subjected to a magnetic field (Sandgren and Snowball, 2001). This might explain the relatively low surface MS signal in the cores; but nevertheless, the main trends in MS seem to co-vary with the other indicators of detrital input (e.g. DBD and XRF Ti count rates, see Fig. 4A and B).

### 4.3. Geochemistry

Most of the geochemical elements included in this study show similar trends to that of Ti. Notable exceptions are the redox-sensitive elements Fe and Mn, which reflect a different pattern of variability than the other geochemical proxies in unit E of GRØP-212. On the other hand, Fe co-varies with the other geochemical proxies in GRØP-312, whereas Mn differs strongly throughout most of that core (see Section 4.5 for a closer description). See Fig. 4 for a compilation of selected physical and geochemical variables from cores GRØP-212 and GRØP-312, where event layers are highlighted in brown.

### 4.4. Age-depth relationships

Chronologies have been established for both piston cores from Grøndalsvatnet (GRØP-212 and GRØP-312) based on AMS radiocarbon ages and $^{210}$Pb ages transferred from GRØS-212 through visual correlation based on the measured physical and geochemical proxies (see Table 1 for radiocarbon ages; Table S1 for $^{210}$Pb ages). Age-depth relationships produced in 'clam' (v. 2.2; Blaauw (2010)), using the IntCal13 calibration curve from Reimer et al. (2013), are shown for cores GRØP-212 and GRØP-312 in Fig. 5A and B, respectively. Ages are not extrapolated beyond the lowermost dated depths (GRØP-212: 230.5 cm; GRØP-312: 156.5 cm). Outliers that showed inverted or future ages were omitted from the age-depth relationships and are shown in red in the figures. In Fig. 5C, the $^{210}$Pb age profile for GRØS-212 is shown with a dark grey shading marking a ± 8.5 year uncertainty, which is added here because $^{137}$Cs peaks indicates that up to ~1 cm of the uppermost

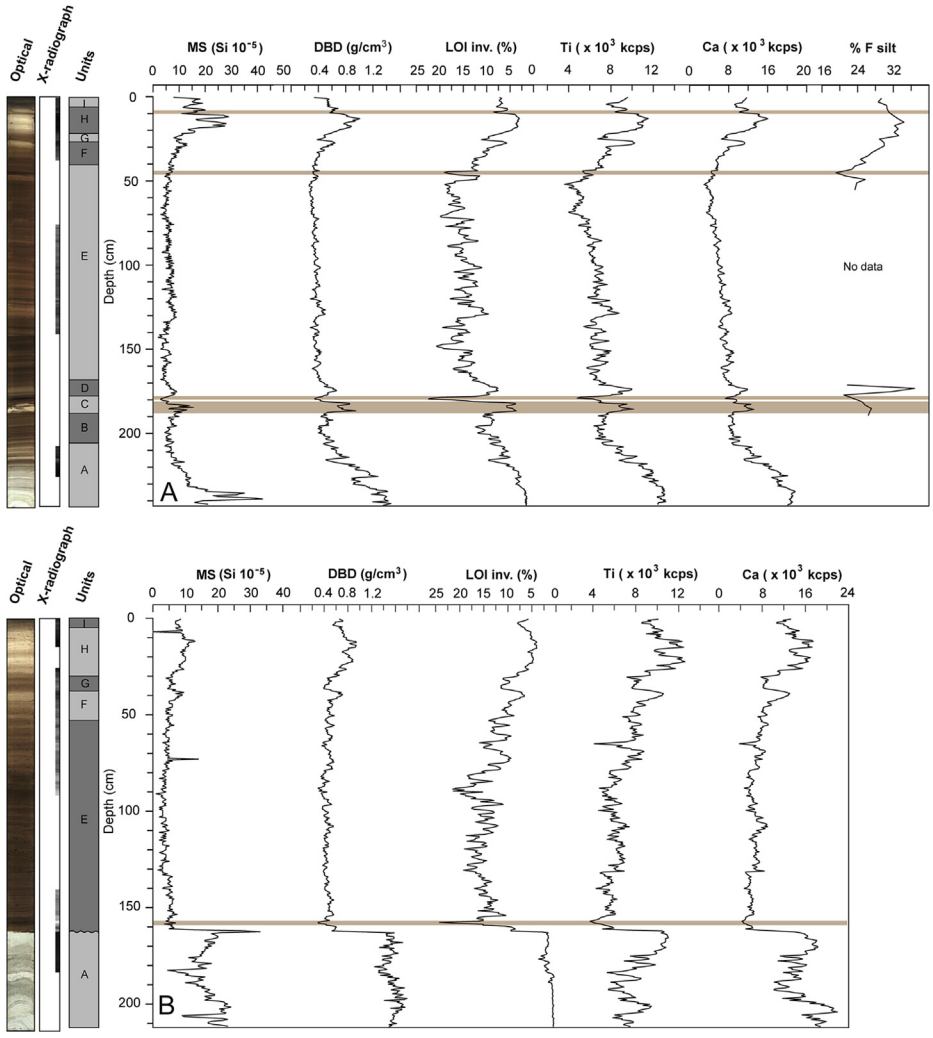


**Fig. 4.** Selected sediment variables from A) GRØP-212; and B) GRØP-312. Line-scan images, radiographic images and lithostratigraphy are shown to the left. Event layers are marked in brown. All data smoothed to 0.5 cm except grain size data from GRØP-212 (2-cm resolution). (For interpretation of the references to colour in this figure legend, the reader is referred to the web version of this article.)

sediment may have been lost during coring (1 cm = ~17 years), while the additional light grey shading marks the regular laboratory uncertainty of the $^{210}$Pb measurements. An independent age-depth relationship was also constructed for STØS-214 using $^{210}$Pb (Fig. S4, see Table S2 for $^{210}$Pb ages). A composite age-model for GRØS-212 was constructed, where ages below the $^{210}$Pb dates were obtained by tuning the GRØS-212 Ti record against the radiocarbon dated GRØP-212 (Fig. 5D). This age-depth relationship is the one used for calibrating the lake sediment data against the ELA-model and in the reconstructions of Neoglacial ELA and winter precipitation (see Sections 4.7 And 4.8).

### 4.5. Principal Component Analysis

For both GRØP-212 and GRØP-312 the PCA returned only one significant Principal Component (PC) axis that explains 88 and 83%, respectively, of the total variance in the datasets (Supplementary Table S3). In both cores the first PC axis captures well the variability of LogLOI, DBD, MS, Ti, K, Ca, Si, Rb, and Sr (Fig. 6). These variables are all strongly correlated, with LOI being inversely correlated to the others. Fe and Mn show a somewhat different pattern of variability than the other geochemical proxies in GRØP-212, and this difference is captured by the second PC axis (Table S3). While the second PC axis is not significant in this analysis, this does not necessarily mean that the PCA2 signal is not related to an underlying causal process. It does, however, indicate that this signal is much weaker than the main pattern of variability in the dataset (represented by PC axis 1), and that Fe and Mn are also strongly affected by this main signal as reflected in their relatively high scores along PC axis 1 (Table S3). In GRØP-312, which covers a shorter time period than GRØP-212 (c.f. Section 4.4), Fe has a very similar variability to that of all the other geochemical proxies, whereas Mn differs strongly with most of its variability captured by PC axis 2. Down-core PCA1 scores for GRØP-212 and GRØP-312 are shown compared to standardized values of all analysed variables in Fig. 6.

### 4.6. Grain-size analyses

Grain-size analyses were performed for selected intervals of GRØP-212 based on time periods of specific interest (and minerogenic content), which included the Neoglacial period and the '8.2 ka BP Event'/Finse Event. Additionally, the high organic content in unit E makes it less suitable for grain-size analyses, as this makes it more

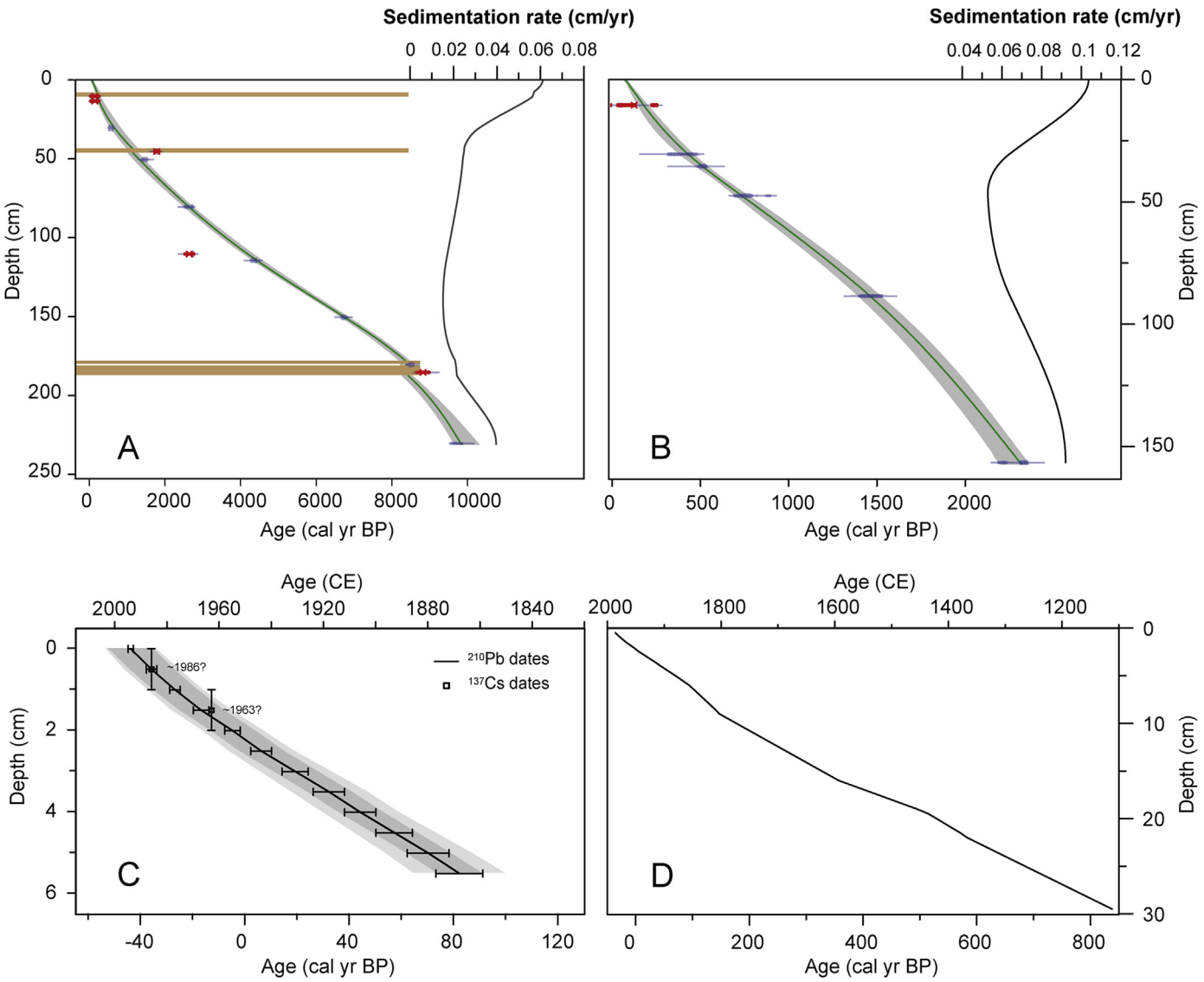


**Fig. 5.** A) Age-depth relationship and sedimentation rate for GRØP-212. Green line is the best estimate smooth spline model age; grey shading marks the 95% (2σ) confidence interval. Blue shaded areas show probability density functions of the calibrated radiocarbon dates. Red shaded areas mark inferred outliers. Horizontal brown layers mark event layer depths. B) Age-depth relationship and sedimentation rate for GRØP-312 (same colour coding as for A). Note the large difference in sedimentation rate compared with GRØP-212. C) $^{210}$Pb age profile for GRØS-212. D) Composite age-depth relationship for GRØS-212, based on $^{210}$Pb ages and $^{137}$Cs ages from GRØS-212, with the lowermost part tuned to the $^{14}$C-based GRØP-212 age-depth relationship. (For interpretation of the references to colour in this figure legend, the reader is referred to the web version of this article.)

challenging to remove all organic material during pre-treatment. Grain-size variations can indicate changes in the amount of glacially eroded rock flour washed into the lake, and in particular, silt fractions can indicate abrasive glacier activity of temperate glaciers (Matthews and Karlén, 1992; Matthews et al., 2000; Nesje et al., 2001; Lie et al., 2004). Of the different grain-size classes, fine silt was found to have the highest co-variance with other indicators of detrital input in GRØP-212 (Fig. 4A).

### *4.7. Calibration of lake record against instrumental data and equilibrium-line altitude reconstructions*

We determined the onset of the local Neoglacial based on variations along PC axis 1 in core GRØP-212 where the trend turns towards increased glacial input at 1400 cal yr BP, and reflects maximum Neoglacial expansion during the LIA (CE1300-1900). In order to reconstruct ELA variations from the lake sediment record, it needs to be calibrated against periods of known or inferred ELA variations. Because moraines are lacking around Ålfotbreen, we applied an ELA model driven by AMO temperature anomalies (Mann et al., 2009) and an index of wintertime westerly geostrophic winds (Nordli et al., 2005) (c.f. Section 3.5). The ELA model could be extended to CE1781 using these data and applied to calibrate the dated lake sediment record covering the same period. In order to get as high temporal resolution as possible, it was desirable to use the ITRAX XRF data for this purpose, and from the PCA it is evident that the elements Ti, Si, K, and Ca all reflect detrital input to the lake, and during the Neoglacial this is inferred to have been driven mainly by glacier activity. Because Ti is insensitive to redox processes (e.g. Croudace et al., 2006) and has previously been shown as a good indicator of glacier erosion (Bakke et al., 2009; Wittmeier et al., 2015), we have used Ti count rates as a glacier proxy, and for the purpose of calibration against modelled ELA, we used the most robustly dated Ti record from GRØS-212. It is expected that the glacier signal captured in the sediments of a distal glacier-fed lake will appear smoothed and lagging behind changes

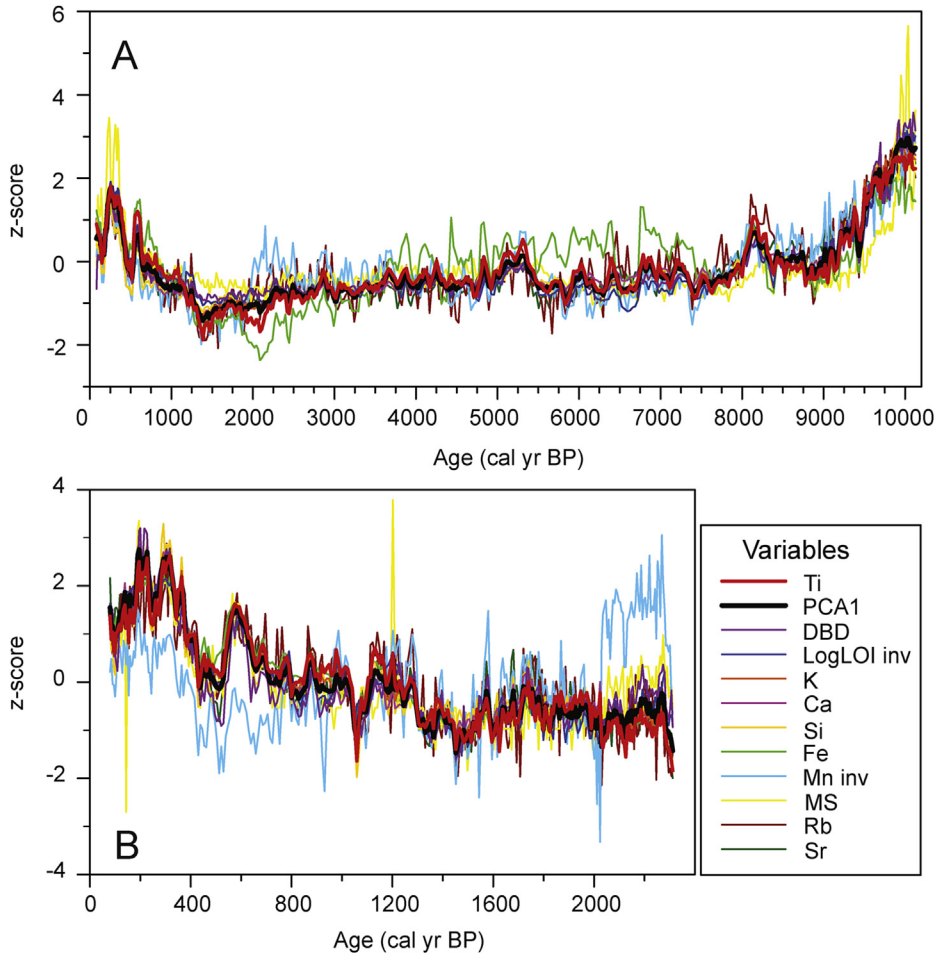


**Fig. 6.** A) Standardized sediment variables and PCA1 scores for GRØP-212. B) Standardized sediment variables and PCA1 scores for GRØP-312. A) and B): LOI is log-transformed and inverted, Mn is inverted. Note how Fe and Mn deviate from the general pattern of variability during certain time periods, and the different age scales between A and B.

in the upstream glacier's ELA due to the response time of the glacier itself and dynamics of the downstream sedimentary system. We performed an autocorrelation between modelled ELA changes and the lake Ti record using Analyseries (Paillard et al., 1996), and obtained the best fit when a lag of 14 years is introduced in the lake record. This lag is within the $^{210}$Pb dating uncertainty (Fig. 5C) before ~ CE1930, whereas in the most recent part of the Ti record an actual lag (i.e. outside the $^{210}$Pb uncertainty range) of up to 4.5 years is required to obtain the maximum fit with the ELA model (Fig. 7). A simple linear regression model was constructed between modelled ELA changes and the Ti record from the GRØS-212 core (Fig. 7). Below the lowermost $^{210}$Pb-date in GRØS-212 we tuned the age-model to the $^{14}$C-dated GRØP-212 using the Ti record, and thus extended the ELA reconstruction to the base of GRØS-212 (Fig. 5D). Beyond this point we applied the same regression model to Ti counts from GRØP-212, although this makes the ELA reconstruction less reliable for this interval because the variability in Ti-counts is slightly different in GRØP-212 than in GRØS-212.

### 4.8. Winter precipitation reconstructions

In order to reconstruct winter precipitation from our reconstructed ELA record, an independent record of summer temperature is needed (c.f. Liestøl in: Sissons, 1979). For this purpose we have calibrated the AMO reconstruction from Mann et al. (2009) against the instrumental summer temperature record in Bergen (using linear regression; $R^2 = 0.78$) and adjusted it for the slight difference in summer temperature (0.15 °C, based on the CE1961-1990 normal period) between Bergen and Sandane (located 30 km east of Ålfotbreen) (Fig. S3). This gives a reconstruction of representative summer temperature for Sandane (Fig. 8 A), which can be used to calculate corresponding temperatures at the changing elevation of the reconstructed ELA of Ålfotbreen (Fig. 8 B) using a lapse rate of 0.65 °C/100 m. Based on the 'Liestøl equation' (eq. (2)), we can then reconstruct winter precipitation (Pw) at the ELA for the entire interval covered by the ELA reconstruction, and finally, the Pw can be adjusted from the variable ELA to a fixed altitude, in this case sea level, using a precipitation reduction of 8%/100 m (c.f. Section 3.6). The reconstructed Pw at sea level is shown in percentage of the modern value (1.7 m water equivalents) in Fig. 8C. Note that both our ELA reconstruction and the temperature record based on the Mann et al. (2009) AMO reconstruction were resampled to a common temporal resolution of 10 years before being used in reconstruction of Pw. While the original AMO reconstruction is available in annual resolution, it does include proxy records that are not annually resolved and the authors of that study state that variability below decadal scales may not necessarily reflect a meaningful climate signal (Mann et al., 2009). Similarly, we assume that due to the response time of the glacier and downstream sedimentary system, the Ti record from Grøndalsvatnet is probably not able to resolve glacier fluctuations below decadal scales.

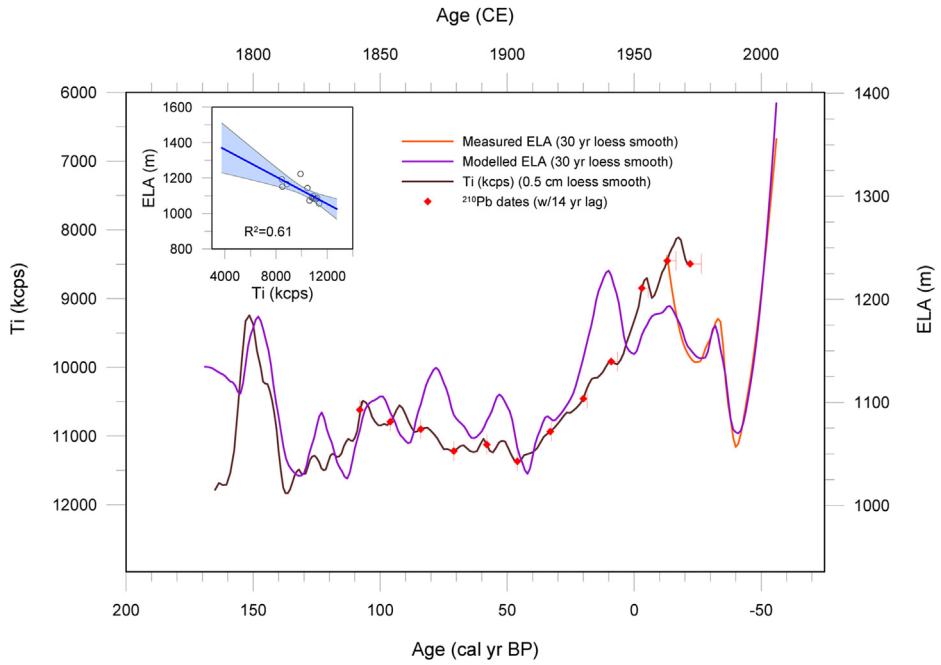


**Fig. 7.** Measured (orange) and modelled (purple) ELA of Ålfotbreen plotted against variations in Ti count rates from the GRØS-212 core (brown). Ti is plotted with a 14-year lag, which gave the best fit against the ELA model. Red points represent $^{210}$Pb-dated levels in the core with error bars showing the minimum lag needed to obtain the optimal fit after accounting for uncertainties in the $^{210}$Pb dating. A linear regression between Ti counts and modelled ELA is shown in the inset figure with 95% confidence bands shaded blue. This regression model was used to reconstruct ELA changes further back in time (Figs. 8 and 10) using the Ti record from GRØS-212 and GRØP-212 (see Section 4.7 for details). (For interpretation of the references to colour in this figure legend, the reader is referred to the web version of this article.)

The central estimates of our reconstructed winter precipitation (Fig. 8C) vary between approximately 55% and 150% of present-day values. Note that the width of the 95% and 68% confidence bands vary between 15% and 115%, and 7%–60%, respectively (see Section 5.3 for discussion of uncertainties). This range of variability in decadal-scale precipitation over the last ~1400 years does not seem unlikely; as a comparison the 10-year average precipitation in Bergen increased from 85% to 125% of the CE1961-1990 mean in the period between CE1960 and CE1995 (data: Norwegian Meteorological Institute; eklima.met.no).

## 5. Discussion

The main objective of this study has been to reconstruct Holocene glacier fluctuations and convert sediment parameters into a quantitative ELA reconstruction that could be further used to calculate past winter precipitation at the Ålfotbreen ice cap. In the following discussion we first assess the utilization of lake sediments for this purpose, and the methodologies applied are evaluated. Second, the results are discussed; first in a broad, Holocene climatic context; and thereafter in the context of Neoglacial ELA variations and winter precipitation. Finally, the results are discussed and compared with relevant climate records from the North Atlantic region, and implications regarding climatic forcing of the Ålfotbreen record are assessed.

### 5.1. Interpretation and application of lake sediments

While lake sediments are valuable palaeoclimatic archives, it is important to be aware of potential sources of error when interpreting these records in a climatic context (Nesje et al., 2004). Instantaneously deposited layers are important to exclude from age-depth modelling, as they might produce erroneous ages and perturb the accumulation rates that result from the age-depth relationship (Rubensdotter and Rosqvist, 2009). As discussed in Section 4.1, we omitted all identified event layers before age-depth relationships were established. Additionally, another possible source of error when studying lake sediments; and in particular proglacial lake sediments, is reworking of older glacigenic sediments (Ballantyne, 2002; Carrivick and Tweed, 2013). However, for small catchments this 'paraglacial' effect will be most significant for a relatively short time period after deglaciation. Provenance studies also indicate that magnetic and geochemical properties of older glacial deposits change over time due to weathering and soil formation (e.g. Vasskog et al., 2012; Wittmeier et al., 2015). Due to the resistant, acidic bedrock in the area (sandstones/conglomerates) superficial deposits are scarce and covered by vegetation in the few places where it is found (mainly the inlet delta and the colluvial fan), meaning that there is generally very little unconsolidated material of non-glacial origin available for erosion in the catchment of Grøndalsvatnet. Input of glacial sediments should therefore, due to the highly effective nature of glacial erosion, be able to dominate the minerogenic sedimentation budget in Grøndalsvatnet when Ålfotbreen is present. Human activities could possibly cause a bias in minerogenic sedimentation, e.g. due to forest clearance and establishment of farmland (e.g. Augustsson et al., 2013). Such effects are difficult to quantify, however, and here we attempt to take such potential biases into account by including a wide confidence range in our final results, as discussed further in Sections 5.2.2 and 5.2.3.

The high correspondence between most of the geochemical elements and the common indicators of detrital input; LogLOI (inverse), MS, and DBD; indicates that the main signal recorded by PC axis 1 in the cores from Grøndalsvatnet reflects the balance between minerogenic and organic content (and water content) in the sediment. This balance is mainly controlled by detrital input from the catchment on one side, and a combination of input of organic detritus from the catchment and organic productivity

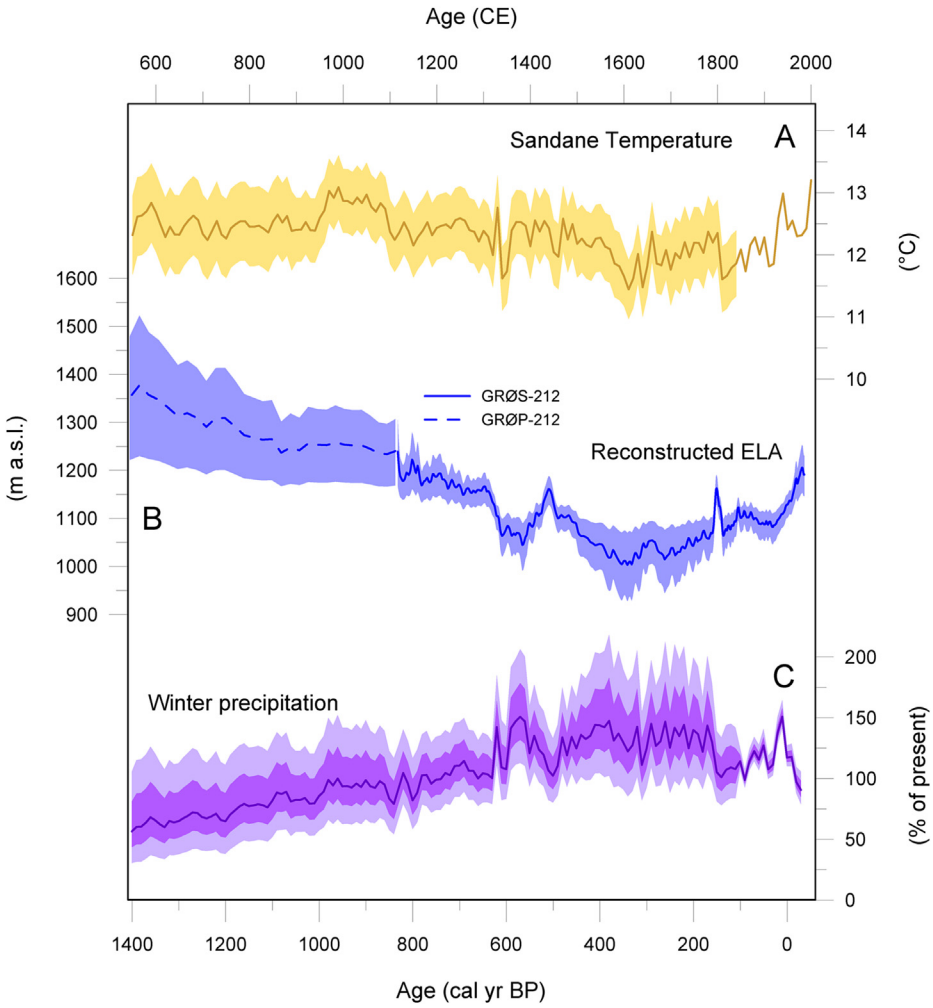


**Fig. 8.** A) Reconstructed Sandane Ts at sea level, adjusted from the regression between Bergen temperatures and the AMO; B) Reconstructed ELA for Ålfotbreen; C) Reconstructed winter precipitation adjusted to sea level. All plots shaded with 95% confidence bands (until start of instrumental period). Winter precipitation is also shown with 68% confidence band.

within the lake itself on the other. These factors may vary independently over time due to e.g. changes in climate and vegetation (input of organic detritus), lake trophic state (internal organic production), or sediment availability (detrital input). The only elements showing signals significantly different from the one captured by PCA1 are Fe and Mn, and this may be explained by their susceptibility to redox processes, both in the catchment or within the lake (Davison, 1993; Naeher et al., 2013). Because of the sparse sedimentary cover in the catchment area, we argue that when the Ålfotbreen ice cap is present, it will probably provide a significant part of the minerogenic input to Grøndalsvatnet through glacial erosion and downstream transport of the resulting glacial flour. Fe and Mn has a higher co-variability with the other parameters from 10,000–7500 cal yr BP and after 1400 cal yr BP in GRØP-212 (Fig. 6). A possible interpretation of this pattern is that increased input of minerogenic material from the glacier will also overprint the effect of redox processes on the deposition of Fe and Mn when the glacier is present.

In all, we conclude that the PCA1 signal reflects detrital input to Grøndalsvatnet, and may thus also give an indication of when the Ålfotbreen glacier has been present in the catchment (Fig. 6). Following deglaciation (~10,100–~9700 cal yr BP) we observe distinct phases of increased PCA1 values centred around 8200 cal yr BP and 5300 cal yr BP, in addition to the period from ~1400 cal yr BP (CE550) until present. The distinct reversal of the PCA1 trend at ~1400 cal yr BP is interpreted as the onset of the Neoglacial period in the study area, after which the glacier has most likely existed continuously until the present. It is not possible to determine for certain from our data whether the glacier was completely melted away during the periods of reduced minerogenic input or just strongly reduced in size (see Section 5.2.1). Furthermore, from relative variations in the sedimentary signal within the Neoglacial, we conclude that the LIA lasted from ~650 cal yr BP (CE1300) until ~50 cal yr BP (CE1900) at Ålfotbreen, with a pronounced glacial maximum between ~400 and 200 cal yr BP (CE1550-1750).

From the age-depth relationships (Fig. 5), and correlation between the cores (Fig. 3), it is apparent that GRØP-212 and GRØP-312 have quite large differences (one order of magnitude) in sediment accumulation rates. The main sedimentary signal recorded by the two cores are very similar over the past ~2300 years (Fig. 6); however, the lower-resolution data from the GRØP-212 coring site was preferred for the further analysis because it covers a longer continuous time period (without any hiatus), and because the $^{210}$Pb dating of the upper part of the record allows calibration against instrumental data at this coring site (Section 4.7). By correlating variations in XRF Ti counts, we found that the lowermost $^{210}$Pb date from GRØS-212 corresponds to the very top of GRØP-212, where some sediment was lost during coring. The obtained $^{210}$Pb dates

from the Støylsvatnet core (STØS-214) do not cover the LIA, but the near linear sedimentation rate determined for the upper 6.5 cm may be extrapolated with some confidence down to the strong increase in Ti counts at ~12 cm. Below this level the peaks in Ti counts indicate an increased detrital input and thus most probably increased sedimentation rates, and these peaks have been correlated to the Ti record in GRØS-212 and GRØP-212 (Fig. 3). We infer that the small ice patch southwest of Blåbreen that currently drains into Svartedalsvatnet must have expanded into the catchment of Støylsvatnet (Fig. 1) at the time represented by these Ti-peaks, and conclude that it was probably retreating from its maximum LIA position at 12 cm depth in the STØS-214 core, which corresponds to approximately CE1720 (Supplementary Fig. S4B).

### 5.2. Holocene glacier fluctuations at Ålfotbreen

#### 5.2.1. Glacier fluctuations in the early to mid-Holocene

Fig. 9 shows the reconstructed relative Holocene glacier variations of Ålfotbreen, as represented by the PCA1 record from core GRØP-212, compared with relevant proxy records from the North Atlantic region.

The timing of deglaciation for Ålfotbreen is concurrent with the end of the 'Erdalen Event II' (e.g. Nesje et al., 2008; Nesje, 2009); a period with glacier advance at Jostedalsbreen, interpreted as a response to colder temperatures around 9700 cal yr BP (Dahl et al., 2002). Weakening laminations upwards in Unit B might reflect a decreasing influx of glacially-eroded sediments, or reworking of paraglacial sediments following this glacier event. If the deglaciation of Ålfotbreen occurred after the 'Erdalen Event II', this shows a regional consistency and coeval glacier retreat in the region encompassing Ålfotbreen and Jostedalsbreen ice caps. Centred around 8200 cal yr BP, there is a marked increase in minerogenic input (Fig. 9E); synchronous with the timing of the '8.2 ka BP Event' recorded in ice cores from Greenland (Fig. 9A) (Rasmussen et al., 2006; Vinther et al., 2006), known as the 'Finse event' in Norway (Nesje and Dahl, 1991; Dahl and Nesje, 1994; Nesje et al., 2008; Nesje, 2009), and a cooling seen in reconstructed July temperature at the nearby Kråkenes site (Fig. 9D; Sylvia M. Peglar and H.J.B. Birks unpublished data). Hormes et al. (2009) found

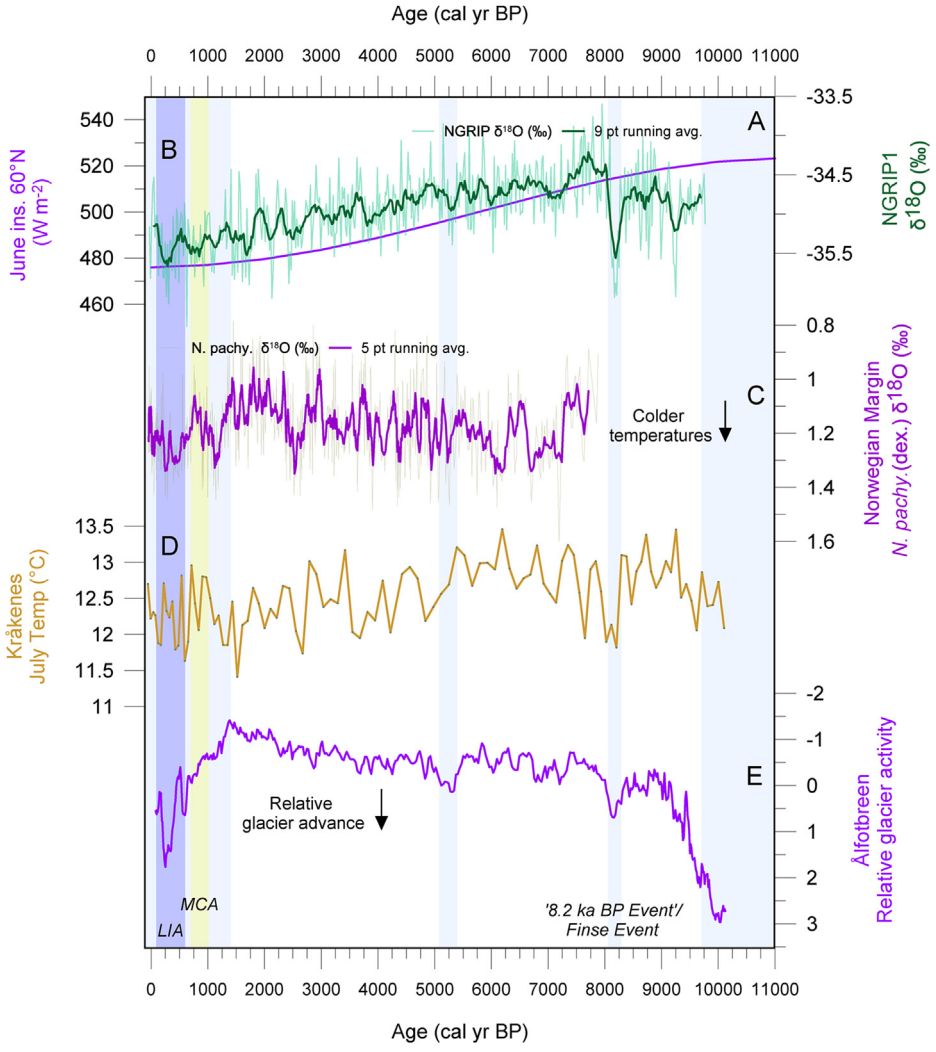


**Fig. 9.** Comparison of reconstructed Holocene glacial activity of E) Ålfotbreen (PCA1; this study) with oxygen isotope records from A) NGRIP (Rasmussen et al., 2006; Vinther et al., 2006); B) June insolation curve for 60 °N (Berger and Loutre, 1991); C) Foraminiferal SST oxygen isotope records from the Norwegian Margin (Sejrup et al., 2011); and D) Kråkenes July Temperature (°C) (Sylvia M. Peglar and H.J.B. Birks, unpublished data). Proxy data are plotted according to latitude with increasing latitude upwards. Light blue shaded areas mark times of possible glacier advances that are discussed in Section 5.2.1, including onset of the Neoglacial at Ålfotbreen. Yellow shaded area marks the Medieval Climatic Anomaly (MCA; 1000–700 cal yr BP), and darker blue shaded area marks the LIA (600–100 cal yr BP); definitions of MCA and LIA from IPCC (2013) and Solomina et al. (2015). (For interpretation of the references to colour in this figure legend, the reader is referred to the web version of this article.)

three glacial events recorded in Nedre Hervavatnet in Sognefjell, western Norway, at 9200, 8600 and 8200 cal yr BP superimposed on a long-term glacier retreat between 9700 and 8000 cal yr BP. It seems likely that the increased input of minerogenic material to Grøndalsvatnet around 8200 cal yr BP might reflect an advance of the Ålfotbreen glacier initiated by colder conditions, or possibly the glacier reformed during this period after having been absent for ~1500 years after deglaciation. See Supplementary Fig. S5 for a comparison of the Ålfotbreen record with NGRIP oxygen isotopes and LOI (i.e., inverted glacier activity) records from Norway from 9500 to 6000 cal yr BP.

From ~8200 to ~5400 cal yr BP, the minerogenic input to Grøndalsvatnet fluctuates, but it is not possible to conclude whether this is related to glacier variability or if the glacier had melted away and the observed fluctuations simply reflect variations in the influx of paraglacial or non-glacial detrital material and organic input/internal productivity in the lake. From ~5400 to 5100 cal yr BP, a relatively strong increase in detrital input is recognized in the record (Fig. 9E), and we suggest that this reflects a period of glacier advance for Ålfotbreen. Following the possible glacier events centred around 8200 and 5300 cal yr BP, the minerogenic content of the core decreases until ~1400 cal yr BP. We suggest that the most likely explanation for the reversal of this trend around 1400 cal yr BP is due to the glacier reforming at the onset of the Neoglacial.

#### 5.2.2. Neoglacial and 'Little Ice Age' variations in equilibrium-line altitude

In Fig. 10 we present the reconstructed high-resolution Neoglacial ELA variations at Ålfotbreen compared with glacier records from Norway and Svalbard, in a south-to-north transect and reconstructed AMO temperature anomalies. Our composite (GRØS-212 and GRØP-212) reconstructed ELA curve suggests that Ålfotbreen could have formed around CE750 (1400 cal yr BP) when the reconstructed ELA is lowered below the top of the present day glacier, and that it may have reached an extent similar to today's around CE1125 (825 cal yr BP) (Fig. 10E). During the LIA maximum (~CE1550-1750), our reconstruction suggests an ELA lowering of ~200 m relative to the present steady-state ELA at ~1180 m.

Interestingly, we observe that the LIA maximum extent period of the individual ice caps/glaciers seems to occur progressively later as we move northwards along the Norwegian coast (indicated by stippled line in Fig. 10). Potential climatic implications of this are discussed in Section 5.4.2.

### 5.3. Past winter precipitation at Ålfotbreen

A proper quantification of the uncertainties in the reconstructed Pw is hard to obtain. For instance, we do not have any quantitative measurement errors for the ITRAX XRF data used in the ELA reconstruction, and there are several potential biases in our record that are hard to quantify, e.g. the effect of forest clearance by humans and changes in land use on the delta plain over the calibration period of our ELA reconstruction, and general changes in input of non-glacial minerogenic material. Instead of a quantitative measure of uncertainty, we therefore present the 95% confidence bands in our ELA reconstruction, as calculated for the linear regression model between Ti counts and modelled ELA (Fig. 8). Mann et al. (2009) estimated 95% uncertainty intervals for their AMO reconstruction, and we have transferred these directly to our reconstructed Sandane temperature record without adding any additional uncertainty arising from the regression procedure against the instrumental temperatures (Supplementary Fig. S3). The final Pw reconstruction is therefore presented with a light shaded band showing the maximum and minimum estimates obtained using the 95% uncertainty interval of the temperature reconstruction and the 95% confidence bands of the ELA reconstruction, and a darker shading to indicate the combined 68% confidence bands (Fig. 8). From CE1860 until present the AMO values are based on instrumental data and for this interval we do not use any uncertainty in temperature. We therefore stress that the final confidence bands shown in Fig. 8C do not represent quantitative uncertainty estimates, but it gives some impression of how confident we can be in interpreting changes in the final reconstructed Pw at different times. Regarding age uncertainties, the age control of the youngest (younger than ~ CE1850) time period is based on $^{210}$Pb ages which yield an uncertainty of ~±10 years. Before ~ CE1850, the radiocarbon age uncertainties are ranging from ±10–100 years, increasing with age down-core.

#### 5.3.1. Comparing reconstructed winter precipitation at Ålfotbreen with records from ice caps in SW Norway

The extreme maritime setting of Ålfotbreen makes reconstructions of past glacier fluctuations and precipitation from this ice cap interesting with respect to how maritime glaciers will respond to projected future increases in both summer temperature and winter precipitation. Precipitation is projected to increase with global rise in temperatures, but this increase is very unlikely to compensate for the effect of increasing temperatures on glacier mass balance (IPCC, 2013). Because ~80% of the net mass balance of Ålfotbreen is presently controlled by (accumulation-season) precipitation (Bn/Bw: $R^2 = 0.76$; Nesje et al. (2000a)), it is interesting to investigate if this relationship holds true also for the past. By doing a simple regression analysis, we find that the Sandane summer temperature record (based on AMO temperature anomalies) explains 32% of the variability in our reconstructed ELA record ($R^2 = 0.32$). By default, the reconstructed Pw record will then explain the remaining 68% ($R^2 = 0.68$), as it is a direct function of the summer temperature and ELA (c.f. the 'Liestøl equation'). It should be noted that the AMO is used as a predictor in the ELA model that was used to transform our Ti measurements to ELA. However, because the transformation is simply linear, it will not serve to falsely increase the correlation between reconstructed ELA and the AMO record (i.e. a correlation against uncalibrated Ti counts will give the same result). Doing a similar analysis of measured mass-balance and ELA on Ålfotbreen between CE1963 and 2010 we find that ablation-season mass-balance explains ~40% of variations in the ELA and winter balance explains ~60%. However, the relative importance of winter and summer balance might change over longer timescales (Trachsel and Nesje, 2015), and we are not able to distinguish any such temporal changes from our reconstruction.

As shown in Fig. 11A, the latest half of our high-resolution dataset of reconstructed Pw (CE550-1980) at Ålfotbreen shows a high degree of similarity with Pw reconstructions at other (maritime) glaciers in SW Norway. The highest degree of covariance is found with the Folgefonna record (Bakke et al., 2005), which is expected, as this record is also highly influenced by maritime conditions and the strength and position of the westerlies. Due to the higher resolution of our record, it is not possible to correlate decadal-scale Pw fluctuations with the other records, but the main trends are similar from ~CE1300 until present. Before CE1300, there is a large discrepancy in the main trend of our record compared to the other Pw records. Part of this difference may be explained by the fact that precipitation reconstructions based on the 'Liestøl equation' are very sensitive to differences in the temperature records applied, as shown in

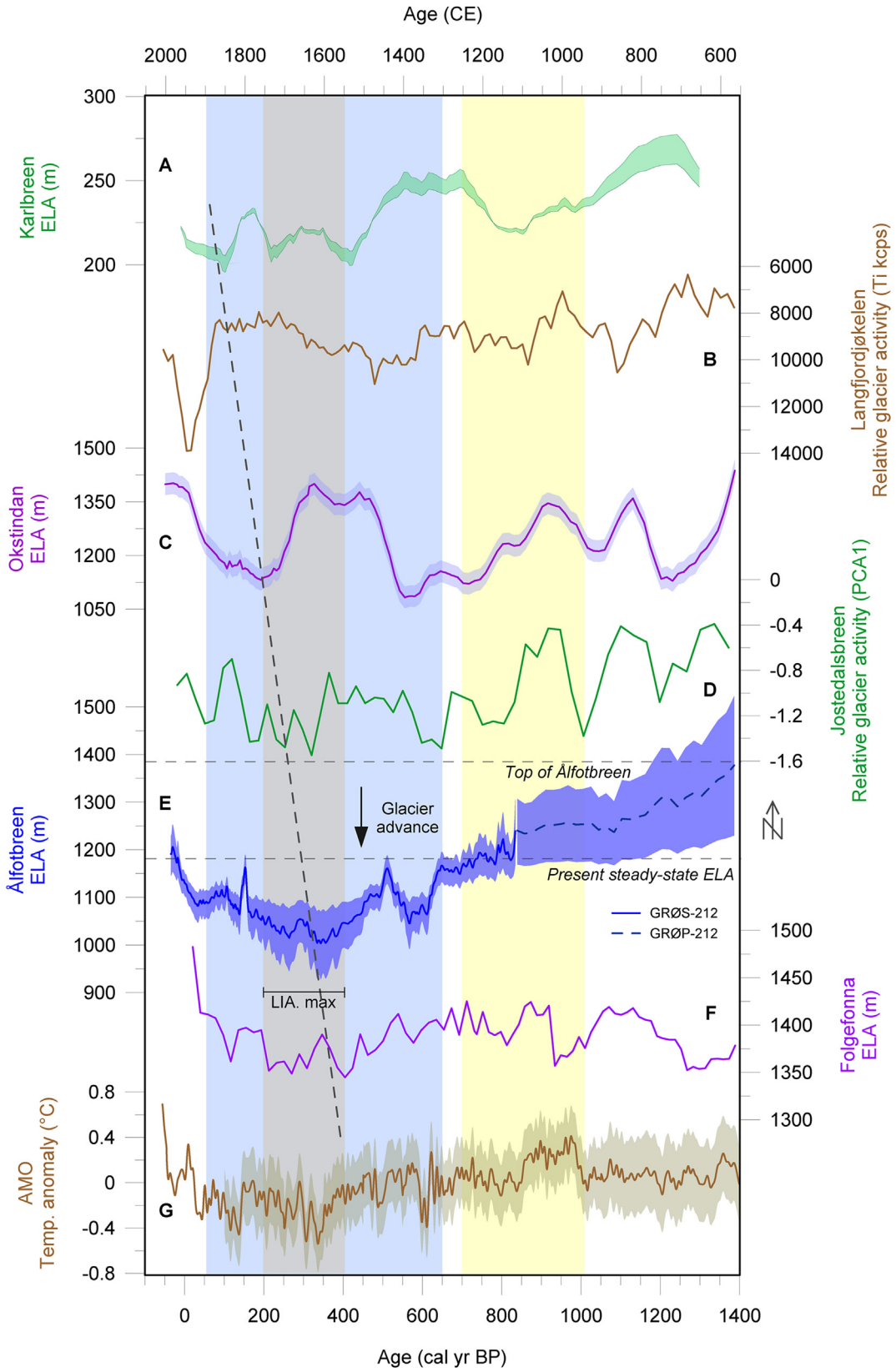


**Fig. 10.** Neoglacial ELA variations at Ålfotbreen (E; this study) compared with A) ELA variations at Karlbreen, NW Svalbard (Røthe et al., 2015); B) Relative glacier activity at Langfjordjøkelen, Arctic Norway (Wittmeier et al., 2015); C) ELA variations at Okstindan, Northern Norway (Bakke et al., 2010); D) Relative glacier activity at Jostedalsbreen, Western Norway (Vasskog et al., 2012); F) ELA variations at Folgefonna, SW Norway (Bakke et al., 2005); and G) Reconstructed AMO temperature anomalies (Mann et al., 2009). Ålfotbreen ELA variations are shown with 95% confidence bands. Light blue shaded vertical area marks the LIA at Ålfotbreen (~650–50 cal yr BP); yellow shaded vertical area marks the MCA (~1000–700 cal yr BP) (following definitions in: IPCC, 2013; Solomina et al., 2015). Light grey shaded vertical area marks the maximum LIA extent at Ålfotbreen (~400–200 cal yr BP). In Supplementary Fig. S6 a similar compilation covering the entire Holocene is shown. (For interpretation of the references to colour in this figure legend, the reader is referred to the web version of this article.)

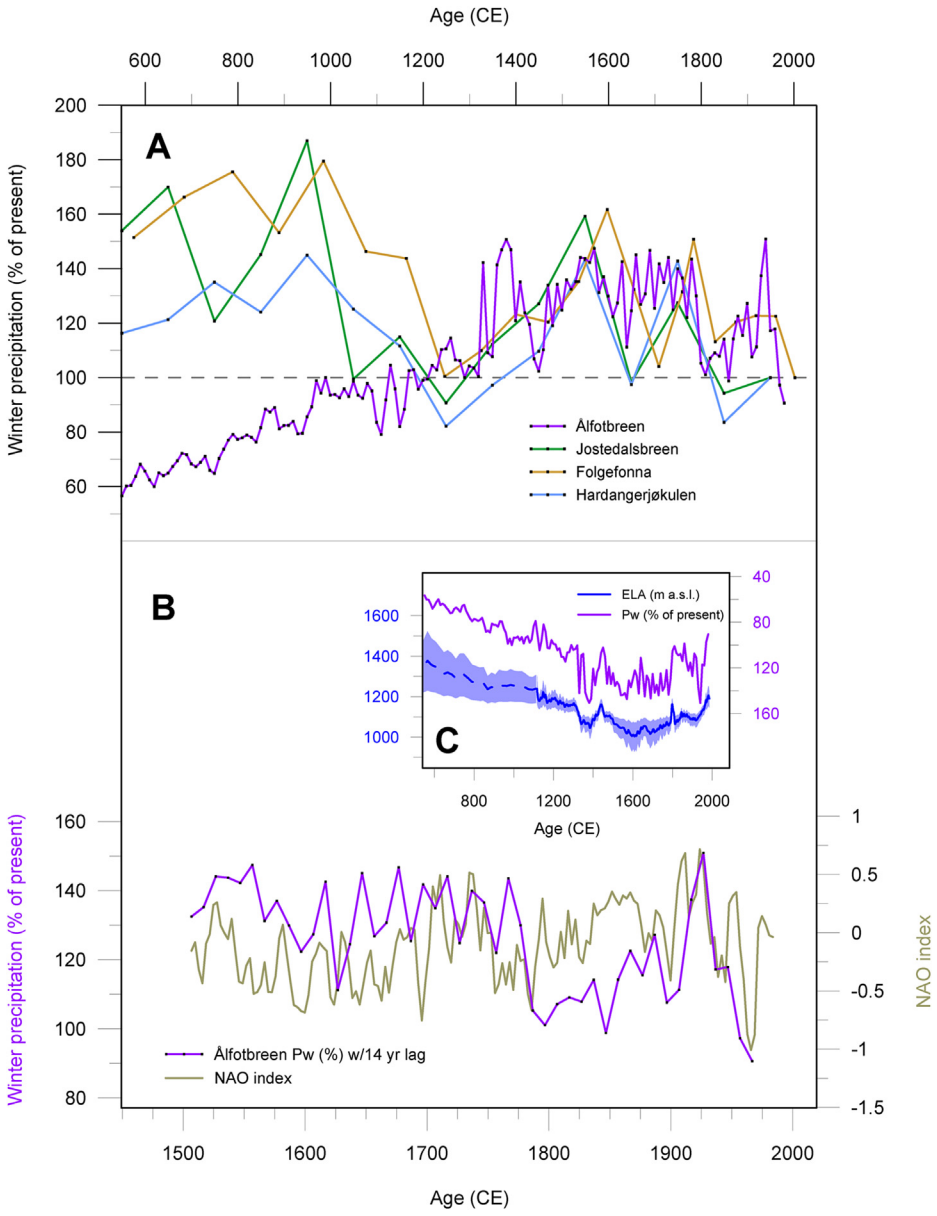


**Fig. 11.** A) Reconstructed winter precipitation (% of present) from Ålfotbreen compared with reconstructed Pw from Jostedalsbreen (Nesje et al., 2001), Folgefonna (Bakke et al., 2005), and Hardangerjøkulen (Dahl and Nesje, 1996). Reference line (stippled) marks present winter precipitation (100%). B) Reconstructed winter precipitation from Ålfotbreen compared with the NAO index from Luterbacher et al. (2001), accounting for a 14-year lag (see Section 4.7). Note change in age scale from A). C) Reconstructed ELA vs. reconstructed Pw (inverted).

Bjune et al. (2005). The pollen record from Vestre Øykjamyrtjørn, which was implemented in the studies from Jostedalsbreen, Folgefonna and Hardangerjøkulen, shows remarkably stable temperatures over the last 4000 years (Bjune et al., 2005), where many other Norwegian records reflect a cooling trend similar to the Kråkenes site (Fig. 9D) and reconstructed AMO (Fig. 10G). This might explain some of the discrepancy between the precipitation reconstructions from the other ice caps and Ålfotbreen before CE1300, although it should also be noted that this is the most uncertain part of our reconstruction. Our record indicates Pw values below present levels before ~CE1200, after which they increase rapidly and remain above present values until near present (Fig. 11A). Values above 130% of present Pw are found close to ~CE1350, 1540, between 1650 and 1770, and at ~CE1930. As winter precipitation along the western coast of Norway is strongly related to the North Atlantic westerlies (Nordli et al., 2005), the ELA variations at Ålfotbreen have most likely been influenced by the spatial and temporal variability of the wintertime westerlies in the past. The wintertime westerlies over southern Norway are closely linked with the NAO (e.g. Nordli et al., 2005), and it is therefore possible that our record of past Pw also contains a signal related to past variations in the NAO (see Section 5.4.2). If new data sets of similar resolution become available from other sites along the Norwegian coast in the future, it will be possible to reconstruct spatiotemporal patterns of winter precipitation, which may help to elucidate past changes in atmospheric circulation patterns (e.g. the NAO) and the strength and position of the wintertime westerlies over Norway. See Supplementary Fig. S7 for mass-balance data from Ålfotbreen compared with the NAO index.

### 5.4. Climatic implications and comparison with northern hemisphere climate records

#### 5.4.1. Deglaciation and early to mid-Holocene glacier fluctuations at Ålfotbreen

Observed Holocene Northern Hemisphere (NH) glacier trends with small or absent glaciers in the mid-Holocene and onset of the Neoglacial between 6000 and 4000 cal yr BP are commonly attributed to decreasing summer temperatures forced by orbitally-controlled insolation changes (Mayewski et al., 2004; Solomina et al., 2015) (Fig. 9B). The resulting NH summer-season cooling caused a progressive southward shift of the NH summer position of the Intertropical Convergence Zone (ITCZ) during the mid-to late Holocene (Haug et al., 2001; Wanner et al., 2008, 2011). In the case of Ålfotbreen, the relationship between glacier variability and climatic forcing is not straight-forward, and we advocate that different mechanisms might have influenced the ice cap at different times. We propose that the timing of deglaciation at Ålfotbreen was a result of the warmer NH summer temperatures driven by increased summer insolation at that time. We further suggest that our glacier reconstruction record the '8.2 ka BP Event'/Finse Event (Nesje and Dahl, 1991; Dahl and Nesje, 1994, 1996; Nesje et al., 2006); a well-established cooling event in the North Atlantic region which was most likely induced by meltwater pulses (Alley et al., 1997; Alley and Ágústsdóttir, 2005; Nesje et al., 2006; Kobashi et al., 2007; Thomas et al., 2007; Kleiven et al., 2008) and subsequent decline in North Atlantic Deep Water formation (Kleiven et al., 2008). It is unclear if the ice cap melted away completely or if it simply retreated following the glacier advance centred around 8200 cal yr BP, but from ~5400 to 5100 cal yr BP we infer a glacier advance at Ålfotbreen. In the Kråkenes temperature record we also observe the onset of a decreasing temperature trend around this time (Fig. 9D). The timing of this glacier advance at Ålfotbreen corresponds well with periods of glacier advance/onset of the Neoglacial at several other ice caps in Norway; in particular Folgefonna (Bakke et al., 2005) (Suppl. Fig. S6F) and Jostedalsbreen [composite record from Nesje et al. (2001) and Vasskog et al. (2012)] (Suppl. Fig. S6D); two ice caps situated relatively close to Ålfotbreen that are likely to be influenced by similar atmospheric and oceanic forcing. We infer that the decreasing NH June insolation acted as the mechanism responsible for this glacier advance in southern Norway and subsequent onset of the Neoglacial at several ice caps.

#### 5.4.2. The Neoglacial and the 'Little Ice Age' at Ålfotbreen

Both the northern parts of Jostedalsbreen and the Northern Folgefonna ice cap evidently melted away due to the 1.5–2 °C warmer summer temperatures that prevailed in the early-to mid-Holocene subsequent to the Finse Event (Bjune et al., 2005; Nesje et al., 2008), before reforming at ~6100 cal yr BP (Nesje et al., 2001) and ~5200 cal yr BP (Bakke et al., 2005), respectively. The higher elevation could explain an earlier initiation of the Neoglacial at Jostedalsbreen, whereas Northern Folgefonna seems to have reformed more-or-less at the same time as the possible glacier advance at Ålfotbreen between 5100 and 5300 cal yr BP. However, after 5100 cal yr BP the trend reverses at Ålfotbreen, and it may have melted completely until ~1400 cal yr BP (Section 5.2.1), while Jostedalsbreen and Folgefonna on the other hand continued to grow throughout this period (Fig. S6). This mid-to late-Holocene reversal at Ålfotbreen is opposite of what we expect as a result from a gradual summer cooling, which should have induced a response more similar to what is seen at both Folgefonna and Jostedalsbreen. Contrary to the increasing terrestrial Neoglacial activity in Scandinavia, the mid- and late Holocene was relatively warm in marine records retrieved outside Norway (Risebrobakken et al., 2003; Sejrup et al., 2011) (Fig. 9C), and this could have served to further reduce the accumulation season length on Ålfotbreen.

Maritime glaciers in Norway are strongly influenced by winter precipitation and the wintertime westerlies (Ballantyne, 1990; Hurrell, 1995; Nesje et al., 2000a; Bakke et al., 2005; Nordli et al., 2005), and Ålfotbreen in particular has shown a very high correlation ($R^2 = 0.51$) between winter mass balance and the leading mode of atmospheric variability in the North Atlantic; the NAO (Nesje et al., 2000a; Nesje, 2009) (Suppl. Fig. S7). Positive NAO-mode years are reflected in the glacier mass-balance of Ålfotbreen as years with a high positive glacier net mass-balance, whereas negative NAO years are associated with atmospheric blocking, forcing the humid air masses to the south or north of SW Norway leading to prevailing colder temperatures and lower winter precipitation on the glaciers in the maritime western Norway. Hence, NAO fluctuations act as a controlling factor governing the amounts of accumulation on glaciers in SW Norway and Holocene glacier records and ELA reconstructions from these glaciers are considered to contain a signal related to past NAO variations (Nesje et al., 2000a). Fig. 11B shows a comparison between reconstructed Pw from Ålfotbreen with the NAO reconstruction from Luterbacher et al. (2001). We observe that there are similar multidecadal trends in our dataset and the reconstructed NAO, although around CE1770-1800 there is a distinct drop in Pw while the NAO values are increasing steadily. Over the last 30 years instrumental NAO measurements are able to explain almost 80% of the variability in the wintertime westerlies over southern Norway; however, this relationship has not been constant over time. Between CE1840 and present there are several 30-year intervals where the NAO explains less than 35% of observed changes in the westerlies index (Suppl. Fig. S8), and we cannot rule out that this relationship has been even weaker in periods beyond the instrumental record. The opposite trends in the reconstructed Ålfotbreen Pw and the NAO around CE1770-1800 (Fig. 11B) could therefore indicate a weaker link between the NAO and wintertime westerlies over Norway in this period. Another possible explanation is that the distinct decrease in North Atlantic Ocean temperatures indicated by the AMO at this time could have served to reduce the moisture availability, thereby reducing winter accumulation on Ålfotbreen. This potential influence of ocean temperatures on winter precipitation is, however, exceedingly difficult to disentangle from the opposite effect that a colder ocean would have on glacier mass-balance through reduced ablation during summer.

During the Medieval Climatic Anomaly (MCA) from 1000 to 700 cal yr BP (CE950-1250) (Solomina et al., 2015), the climate in the North Atlantic region was relatively warm (e.g. Mann et al., 2009). The ELA of Ålfotbreen shows a steady lowering from the start of our record at CE550 before stabilizing at a level close to its present elevation during most of the MCA (Fig. 10). This implies that reconstructed Pw increases over the same interval, and it is during the MCA that our central estimate of Pw first reaches present-day levels and above (Fig. 11B).

The 'Little Ice Age' was a period of glacier advance across the world, but the mechanisms driving these advances are presently not fully understood (Broecker, 2000; Nesje and Dahl, 2003; Solomina et al., 2015). One of the key issues addressed is defining the exact timing of the LIA, which may vary significantly from site to site depending on the types of proxy records used (e.g. glaciers, temperature, or precipitation) and different climatic settings. The LIA at Ålfotbreen shows a pattern similar to other glacier records from Norway and Svalbard (Fig. 10) with an onset ~650 cal yr BP (CE1300), lasting until ~50 cal yr BP (CE1900). The LIA maximum extent of Ålfotbreen occurred between ~400 and 200 cal yr BP (CE1550-1750). In Fig. 10E, our reconstruction shows an ELA lowering of ~200 m during the LIA relative to the present

steady-state ELA at ~1180 m. This order of magnitude is similar to what we find for e.g. Okstindan in Arctic Norway (Bakke et al., 2010), which showed an ELA lowering of 250 m during the LIA (Fig. 10C).

An interesting time-transgressive trend in the LIA maximum can be observed in Fig. 10: The timing of the LIA maximum tends to occur progressively later as we move northwards (see stippled line). Because temperatures during the LIA are regionally consistent for the area of interest (Mann et al., 2009) we suggest that winter precipitation might be the most important factor controlling the timing of the LIA maximum for the glaciers in this south-north transect. We acknowledge that the compiled glacier reconstructions have significant uncertainties in age control, but the overall difference in timing from north to south is larger than what can be explained by age uncertainty alone. We therefore suggest that the observed progressively later maximum glacier advances are likely forced by regional differences in winter precipitation. From observations we know that regional changes in precipitation in the North Atlantic are strongly linked to the NAO, but there are still large uncertainties in how the NAO has behaved in the past (Lehner et al., 2012; Pinto and Raible, 2012). Proxy reconstructions of the NAO often show widely conflicting results prior to the instrumental record, with some reconstructions suggesting a change to a generally more positive NAO mode during the LIA (e.g. Meeker and Mayewski, 2002), while others indicate the opposite (e.g. Trouet et al., 2009). One challenge in this respect is to distinguish between the effects of strength versus frequency of North Atlantic cyclones on long-term trends in the reconstructed NAO (e.g. Trouet et al., 2012). From the connection between winter mass balance on Ålfotbreen and the NAO, our reconstruction seems to favour a change towards a generally more positive NAO situation during the LIA, but the question of cyclone frequency versus intensity remains. New high-resolution precipitation reconstructions along the coast of Norway might add to our knowledge of past changes in the NAO (Lehner et al., 2012), and reveal whether the time-transgressive northward migration of the LIA glacier maximum is related to this atmospheric circulation feature.

### 5.5. What does the future hold for Ålfotbreen?

Ålfotbreen might become one of the first glaciers in Norway to melt completely if the present warming trend continues without being compensated for by increased accumulation-season precipitation (Nesje et al., 2008; Andreassen et al., 2012). According to an energy-balance modelling study, Ålfotbreen is predicted to respond with an ELA rise of 135 m and a mass balance change of −1.11 m water equivalents (m.w.e.) per year as a response to a 1 °C increase in temperature (Oerlemans, 1992). Temperature projections for the future exceed 1.5 °C of warming (relative to CE1850-1900) by the end of the 21st century (IPCC, 2013), which is similar in magnitude to peak warming during the Holocene Thermal Maximum (Seppä and Birks, 2001; Davis et al., 2003; Renssen et al., 2009). As our record shows that Ålfotbreen was most likely melted away during this period (from 8200 to ~5400 cal yr BP) we infer that Ålfotbreen might melt away completely within the end of the 21st century. If a positive NAO mode were to prevail along with cooler summer temperatures for several years, this could lead to an expansion of the Ålfotbreen ice cap; however, the current warming trend is expected to continue, and the future variability of the NAO is not possible to predict. If the ice cap should melt away completely within the end of the 21st century, as our current best knowledge seems to suggest, this will be the first time in more than 1400 years that the Ålfotbreen mountain plateau becomes entirely ice-free.

## 6. Conclusions

In a future warmer climate, Ålfotbreen is one of the most vulnerable glaciers in Norway and the ice cap might disappear completely within few decades due to its narrow hypsometry and low altitude. Here we have presented and assessed novel data on past variations of Ålfotbreen, including periods where the glacier might have been totally melted away. We have focused in particular on the Neoglacial period with high-resolution reconstructions of ELA variations and winter precipitation covering the last ~1400 years. Our results can be summarized as follows:

(1) Ålfotbreen retreated/melted away between ca. 10,100–9700 cal yr BP, following deglaciation. The ice cap reformed and/or experienced a glacier advance during the '8.2 ka BP Event'/Finse event (centred ~8200 cal yr BP). Thereafter, the ice cap probably melted away completely until a possible new glacier advance is recorded from ca. 5400–5100 cal yr BP. The timing of this advance is approximately synchronous with other glacier advances in western Norway at the Jostedalsbreen and Folgefonna ice caps. Following this glacier event, the ice cap probably melted away completely again and did not reform until the onset of the local Neoglacial period at ~1400 cal yr BP. The LIA is determined to have lasted from ~650 cal yr BP (CE1300) until ~50 cal yr BP (CE1900), with the LIA maximum occurring from ~400 to 200 cal yr BP (CE1550-1750). The LIA maximum was probably the largest glacier extent of Ålfotbreen since deglaciation.

(2) A regional synthesis of Neoglacial glacier variations is presented in a south-north transect, showing an apparent time-transgressive trend of the LIA maximum extents with the onset of the LIA seemingly starting progressively later as we move further north. We suggest that this is likely forced by regional winter precipitation differences along the coast of Norway.

(3) Our high-resolution precipitation reconstruction, based on independent Ts and ELA reconstructions, correlates well with other Pw reconstructions from SW Norway after CE1300. Before this (between CE550-1300) the records diverge, possibly due to differences in the summer temperature records used when reconstructing Pw through the 'Liestøl equation'. Our novel approach of calculating ELA and winter precipitation could be applied at other sites where lack of (dated) moraines complicates the accurate timing and extent of past glacier advances, although this requires instrumental measurements of ELA.

## Acknowledgements

This research was supported by the Centre for Climate Dynamics at the Bjerknes Centre for Climate Research and the SHIFTS project funded by the Norwegian Research Council (210004). Gunhild Rosqvist is thanked for helpful comments on earlier drafts of the manuscript. We thank landowner Leidulv Solvang for permission to core Lake Grøndalsvatnet and for providing boats used during fieldwork, and Bjørn André Skjæret for invaluable help with coring. Anne Bjune helped identify terrestrial plant remains for AMS radiocarbon dating. Permission to core Støylsvatnet was granted from Alf Erik Røyrvik and the Norwegian Environment Agency. Magnetic measurements were carried out at the Palaeomagnetic Laboratory at the University of Bergen (under administration of the late Prof. Reidar Løvlie). Radiocarbon dating was carried out at the Poznan Radiocarbon Laboratory under supervision of Tomasz Goslar. Peter Appleby supervised the $^{210}$Pb dating at the

Environmental Radioactivity Research Centre, University of Liverpool. The authors would like to thank an anonymous reviewer for valuable feedback that served to improve the manuscript.

Ålfotbreen ELA and Pw reconstruction dataset is to be deposited in the NOAA data repository.

## Appendix A. Supplementary data

Supplementary data related to this article can be found at http://dx.doi.org/10.1016/j.quascirev.2015.12.004.

## References

Alley, R.B., Ágústsdóttir, A.M., 2005. The 8k event: cause and consequences of a major Holocene abrupt climate change. Quat. Sci. Rev. 24, 1123–1149.
Alley, R.B., Mayewski, P.A., Sowers, T., Stuiver, M., Taylor, K.C., Clark, P.U., 1997. Holocene climatic instability: a prominent, widespread event 8200 yr ago. Geology 25, 483–486.
Andreassen, L., Winsvold, S., Paul, F., Hausberg, J., 2012. Inventory of Norwegian Glaciers. NVE, Oslo.
Andreassen, L.M., Elvehøy, H., Kjollmoen, B., Engeset, R.V., Haakensen, N., 2005. Glacier mass-balance and length variation in Norway. Ann. Glaciol. 42, 317–325.
Augustsson, A., Gaillard, M.-J., Peltola, P., Mazier, F., Bergbäck, B., Saarinen, T., 2013. Effects of land use and climate change on erosion intensity and sediment geochemistry at Lake Lehmilampi, Finland. Holocene, 0959683613484615.
Bakke, J., Dahl, S.O., Paasche, Ø., Riis Simonsen, J., Kvisvik, B., Bakke, K., Nesje, A., 2010. A complete record of Holocene glacier variability at Austre Okstindbreen, northern Norway: an integrated approach. Quat. Sci. Rev. 29, 1246–1262.
Bakke, J., Lie, Ø., Heegaard, E., Dokken, T., Haug, G.H., Birks, H.H., Dulski, P., Nilsen, T., 2009. Rapid oceanic and atmospheric changes during the younger dryas cold period. Nat. Geosci. 2, 202–205.
Bakke, J., Nesje, A., Dahl, S.O., 2005. Utilizing physical sediment variability in glacier-fed lakes for continuous glacier reconstructions during the Holocene, northern Folgefonna, western Norway. The Holocene 15, 161–176.
Bakke, J., Trachsel, M., Kvisvik, B.C., Nesje, A., Lyså, A., 2013. Numerical analyses of a multi-proxy data set from a distal glacier-fed lake, Sørsendalsvatn, western Norway. Quat. Sci. Rev. 73, 182–195.
Ballantyne, C.K., 1989. The Loch Lomond Readvance on the Isle of Skye, Scotland: glacier reconstruction and palaeoclimatic implications. J. Quat. Sci. 4, 95–108.
Ballantyne, C.K., 1990. The Holocene glacial history of Lyngshalvøya, northern Norway: chronology and climatic implications. Boreas 19, 93–117.
Ballantyne, C.K., 2002. Paraglacial geomorphology. Quat. Sci. Rev. 21, 1935–2017.
Berger, A., Loutre, M.-F., 1991. Insolation values for the climate of the last 10 million years. Quat. Sci. Rev. 10, 297–317.
Bjune, A.E., Bakke, J., Nesje, A., Birks, H.J.B., 2005. Holocene mean july temperature and winter precipitation in western Norvay inferred from palynological and glaciological lake-sediment proxies. The Holocene 15, 177–189.
Blaauw, M., 2010. Methods and code for 'classical'age-modelling of radiocarbon sequences. Quat. Geochronol. 5, 512–518.
Blott, S.J., Pye, K., 2001. GRADISTAT: a grain size distribution and statistics package for the analysis of unconsolidated sediments. Earth Surf. Process. Landforms 26, 1237–1248.
Briner, J., Stewart, H., Young, N., Philipps, W., Losee, S., 2010. Using proglacial-threshold lakes to constrain fluctuations of the Jakobshavn Isbræ ice margin, western Greenland, during the Holocene. Quat. Sci. Rev. 29, 3861–3874.
Broecker, W.S., 2000. Was a change in thermohaline circulation responsible for the Little Ice Age? Proc. Natl. Acad. Sci. 97, 1339–1342.
Bryhni, I., Lutro, O., 2000. Berggrunnskart Naustdal 1218 III, M: 1:50.000. NGU.
Carrivick, J.L., Tweed, F.S., 2013. Proglacial lakes: character, behaviour and geological importance. Quat. Sci. Rev. 78, 34–52.
Croudace, I.W., Rindby, A., Rothwell, R.G., 2006. ITRAX: description and evaluation of a new multi-function X-ray core scanner. Special Publ. Geol. Soc. Lond. 267, 51.
Dahl, S.O., Bakke, J., Lie, Ø., Nesje, A., 2003. Reconstruction of former glacier equilibrium-line altitudes based on proglacial sites: an evaluation of approaches and selection of sites. Quat. Sci. Rev. 22, 275–287.
Dahl, S.O., Nesje, A., 1992. Paleoclimatic implications based on equilibrium-line altitude depressions of reconstructed younger dryas and Holocene cirque glaciers in inner Nordfjord, western Norway. Palaeogeogr. Palaeoclimatol. Palaeoecol. 94, 87–97.
Dahl, S.O., Nesje, A., 1994. Holocene glacier fluctuations at Hardangerjøkulen, central-southern Norway: a high-resolution composite chronology from lacustrine and terrestrial deposits. The Holocene 4, 269–277.
Dahl, S.O., Nesje, A., 1996. A new approach to calculating Holocene winter precipitation by combining glacier equilibrium-line altitudes and pine-tree limits: a case study from Hardangerjøkulen, central southern Norway. The Holocene 6, 381–398.
Dahl, S.O., Nesje, A., Lie, Ø., Fjordheim, K., Matthews, J.A., 2002. Timing, equilibrium-line altitudes and climatic implications of two early-Holocene glacier readvances during the Erdalen Event at Jostedalsbreen, western Norway. The Holocene 12, 17–25.
Davis, B., Brewer, S., Stevenson, A., Guiot, J., 2003. The temperature of Europe during the Holocene reconstructed from pollen data. Quat. Sci. Rev. 22, 1701–1716.
Davison, W., 1993. Iron and manganese in lakes. Earth Sci. Rev. 34, 119–163.
Dean, W.E., 1974. Determination of carbonate and organic matter in calcareous sediments and sedimentary rocks by loss on ignition: comparison with other methods. J. Sediment. Res. 44.
Haakensen, N., 1989. Akkumulasjon på breene i Norge vinteren 1988–89. Været 13, 91–94.
Haug, G.H., Hughen, K.A., Sigman, D.M., Peterson, L.C., Röhl, U., 2001. Southward migration of the intertropical convergence zone through the Holocene. Science 293, 1304–1308.
Heiri, O., Lotter, A.F., Lemcke, G., 2001. Loss on ignition as a method for estimating organic and carbonate content in sediments: reproducibility and comparability of results. J. Paleolimnol. 25, 101–110.
Hormes, A., Blaauw, M., Dahl, S.O., Nesje, A., Possnert, G., 2009. Radiocarbon wiggle-match dating of proglacial lake sediments–Implications for the 8.2 ka event. Quat. Geochronol. 4, 267–277.
Hurrell, J.W., 1995. Decadal trends in the North Atlantic oscillation: regional temperatures and precipitation. Science 269, 676.
IPCC, 2013. In: Stocker, T., Qin, D., Plattner, G., Tignor, M., Allen, S., Boschung, J., Nauels, A., Xia, Y., Bex, V., Midgley, P. (Eds.), Climate Change 2013: the Physical Science Basis. Contribution of Working Group I to the Fifth Assessment Report of the Intergovernmental Panel on Climate Change. Cambridge Univ Press, Cambridge, United Kingdom and New York, NY, USA.
Jones, P., Davies, T., Lister, D., Slonosky, V., Jonsson, T., Bärring, L., Jönsson, P., Maheras, P., Kolyva-Machera, F., Barriendos, M., 1999. Monthly mean pressure reconstructions for Europe for the 1780–1995 period. Int. J. Climatol. 19, 347–364.
Karlén, W., 1976. Lacustrine sediments and tree-limit variations as indicators of Holocene climatic fluctuations in Lappland, northern Sweden. Geogr. Ann. Ser. A. Phys. Geogr. 1–34.
Karlén, W., 1981. Lacustrine sediment studies. A technique to obtain a continous record of holocene glacier variations. Geogr. Ann. Ser. A. Phys. Geogr. 273–281.
Karlén, W., Matthews, J.A., 1992. Reconstructing Holocene glacier variations from glacial lake sediments: studies from Nordvestlandet and Jostedalsbreen-Jotunheimen, southern Norway. Geogr. Ann. Ser. A. Phys. Geogr. 327–348.
Kjøllmoen, B., 2011. Glaciological Investigations in Norway in 2010. NVE Report 2 2010.
Kleiven, H.K.F., Kissel, C., Laj, C., Ninnemann, U.S., Richter, T.O., Cortijo, E., 2008. Reduced North Atlantic deep water coeval with the glacial Lake Agassiz freshwater outburst. Science 319, 60–64.
Kobashi, T., Severinghaus, J.P., Brook, E.J., Barnola, J.-M., Grachev, A.M., 2007. Precise timing and characterization of abrupt climate change 8200 years ago from air trapped in polar ice. Quat. Sci. Rev. 26, 1212–1222.
Lehner, F., Raible, C.C., Stocker, T.F., 2012. Testing the robustness of a precipitation proxy-based North Atlantic oscillation reconstruction. Quat. Sci. Rev. 45, 85–94.
Lepš, J., Šmilauer, P., 2003. Multivariate Analysis of Ecological Data Using CANOCO. Cambridge University Press, Cambridge.
Lie, Ø., Dahl, S.O., Nesje, A., Matthews, J.A., Sandvold, S., 2004. Holocene fluctuations of a polythermal glacier in high-alpine eastern Jotunheimen, central-southern Norway. Quat. Sci. Rev. 23, 1925–1945.
Luterbacher, J., Xoplaki, E., Dietrich, D., Jones, P., Davies, T., Portis, D., Gonzalez-Rouco, J., Von Storch, H., Gyalistras, D., Casty, C., 2001. Extending North Atlantic oscillation reconstructions back to 1500. Atmos. Sci. Lett. 2, 114–124.
Mann, M.E., Zhang, Z., Rutherford, S., Bradley, R.S., Hughes, M.K., Shindell, D., Ammann, C., Faluvegi, G., Ni, F., 2009. Global signatures and dynamical origins of the Little Ice Age and medieval climate Anomaly. Science 326, 1256–1260.
Marzeion, B., Nesje, A., 2012. Spatial patterns of North Atlantic oscillation influence on mass balance variability of European glaciers. Cryosphere Discuss. 6, 1–35.
Masson-Delmotte, V., Schulz, M., Abe-Ouchi, A., Beer, J., Ganopolski, A., Rouco, J.G., Jansen, E., Lambeck, K., Luterbacher, J., Naish, T., 2013. Information from paleoclimate archives. In: Stocker, T., Qin, D., Plattner, G., Tignor, M., Allen, S., Boschung, J., Nauels, A., Xia, Y., Bex, V., Midgley, P. (Eds.), Climate Change 2013: the Physical Science Basis. Contribution of Working Group I to the Fifth Assessment Report of the Intergovernmental Panel on Climate Change. Cambridge Univ Press, Cambridge, United Kingdom and New York, NY, USA, pp. 383–464.
Matthews, J.A., Karlén, W., 1992. Asynchronous neoglaciation and Holocene climatic change reconstructed from Norwegian glaciolacustrine sedimentary sequences. Geology 20, 991.
Matthews, J.A., Olaf Dahl, S., Nesje, A., Berrisford, M.S., Andersson, C., 2000. Holocene glacier variations in central Jotunheimen, southern Norway based on distal glaciolacustrine sediment cores. Quat. Sci. Rev. 19, 1625–1647.
Mayewski, P.A., Rohling, E.E., Curt Stager, J., Karlen, W., Maasch, K.A., David Meeker, L., Meyerson, E.A., Gasse, F., van Kreveld, S., Holmgren, K., 2004. Holocene climate variability. Quat. Res. 62, 243–255.
Meeker, L.D., Mayewski, P.A., 2002. A 1400-year high-resolution record of atmospheric circulation over the north Atlantic and Asia. The Holocene 12, 257–266.
Naeher, S., Gilli, A., North, R.P., Hamann, Y., Schubert, C.J., 2013. Tracing bottom water oxygenation with sedimentary Mn/Fe ratios in Lake Zurich, Switzerland. Chem. Geol. 352, 125–133.
Nesje, A., 1992. A piston corer for lacustrine and marine sediments. Arct. Alp. Res. 257–259.
Nesje, A., 2005. Briksdalsbreen in western Norway: AD 1900-2004 frontal

fluctuations as a combined effect of variations in winter precipitation and summer temperature. The Holocene 15, 1245–1252.
Nesje, A., 2009. Latest Pleistocene and Holocene alpine glacier fluctuations in Scandinavia. Quat. Sci. Rev. 28, 2119–2136.
Nesje, A., Bakke, J., Dahl, S.O., Lie, Ø., Bøe, A.-G., 2007. A continuous, high-resolution 8500-yr snow-avalanche record from western Norway. The Holocene 17, 269–277.
Nesje, A., Bakke, J., Dahl, S.O., Lie, Ø., Matthews, J.A., 2008. Norwegian mountain glaciers in the past, present and future. Glob. Planet. Change 60, 10–27.
Nesje, A., Bjune, A.E., Bakke, J., Dahl, S.O., Lie, Ø., Birks, H.J.B., 2006. Holocene palaeoclimate reconstructions at Vanndalsvatnet, western Norway, with particular reference to the 8200 cal. yr BP event. The Holocene 16, 717–729.
Nesje, A., Dahl, S.O., 1991. Holocene glacier variations of Blåisen, Hardangerjøkulen, central southern Norway. Quat. Res. 35, 25–40.
Nesje, A., Dahl, S.O., 2003. The 'Little Ice Age'—only temperature? The Holocene 13, 139–145.
Nesje, A., Dahl, S.O., Bakke, J., 2004. Were abrupt lateglacial and early-Holocene climatic changes in northwest Europe linked to freshwater outbursts to the north Atlantic and Arctic cceans? The Holocene 14, 299–310.
Nesje, A., Dahl, S.O., Løvlie, R., 1995. Late Holocene glaciers and avalanche activity in the Ålfotbreen area, western Norway: evidence from a lacustrine sedimentary record. Nor. Geol. Tidsskr. 75, 120–126.
Nesje, A., Kvamme, M., Rye, N., Løvlie, R., 1991. Holocene glacial and climate history of the Jostedalsbreen region, western Norway; evidence from lake sediments and terrestrial deposits. Quat. Sci. Rev. 10, 87–114.
Nesje, A., Lie, Ø., Dahl, S.O., 2000a. Is the North Atlantic oscillation reflected in Scandinavian glacier mass balance records? J. Quat. Sci. 15, 587–601.
Nesje, A., Matthews, J.A., Dahl, S.O., Berrisford, M.S., Andersson, C., 2001. Holocene glacier fluctuations of Flatebreen and winter-precipitation changes in the Jostedalsbreen region, western Norway, based on glaciolacustrine sediment records. The Holocene 11, 267–280.
Nesje, A., Olaf Dahl, S., Andersson, C., Matthews, J.A., 2000b. The lacustrine sedimentary sequence in Sygneskardvatnet, western Norway: a continuous, high-resolution record of the Jostedalsbreen ice cap during the Holocene. Quat. Sci. Rev. 19, 1047–1065.
Nordli, Ø., Lie, Ø., Nesje, A., Benestad, R.E., 2005. Glacier mass balance in southern Norway modelled by circulation indices and Spring-Summer temperatures ad 1781–2000. Geogr. Ann. Ser. A Phys. Geogr. 87, 431–445.
Oerlemans, J., 1992. Climate sensitivity of glaciers in southern Norway: application of an energy-balance model to Nigardsbreen, Hellstugubreen and Ålfotbreen. J. Glaciol. 38, 223–232.
Oerlemans, J., 2005. Extracting a climate signal from 169 glacier records. Science 308, 675–677.
Paillard, D., Labeyrie, L., Yiou, P., 1996. Macintosh program performs time-series analysis. Eos Trans. Am. Geophys. Union 77, 379–379.
Pinto, J.G., Raible, C.C., 2012. Past and recent changes in the North Atlantic oscillation. Wiley Interdiscip. Rev. Clim. Change 3, 79–90.
R Development Core Team, 2012. R: a Language and Environment for Statistical Computing. R Foundation for Statistical Computing. R Foundation for Statistical Computing, Vienna, Austria.
Rasmussen, S.O., Andersen, K.K., Svensson, A., Steffensen, J.P., Vinther, B.M., Clausen, H.B., Siggaard-Andersen, M.L., Johnsen, S.J., Larsen, L.B., Dahl-Jensen, D., 2006. A new Greenland ice core chronology for the last glacial termination. J. Geophys. Res. Atmos. (1984–2012) 111.
Reimer, P.J., Bard, E., Bayliss, A., Beck, J.W., Blackwell, P.G., Ramsey, C.B., Buck, C.E., Cheng, H., Edwards, R.L., Friedrich, M., 2013. IntCal13 and Marine13 radiocarbon age calibration curves 0–50,000 years cal BP. Radiocarbon 55, 1869–1887.
Renssen, H., Seppä, H., Heiri, O., Roche, D., Goosse, H., Fichefet, T., 2009. The spatial and temporal complexity of the Holocene thermal maximum. Nat. Geosci. 2, 411–414.
Risebrobakken, B., Jansen, E., Andersson, C., Mjelde, E., Hevrøy, K., 2003. A high-resolution study of Holocene paleoclimatic and paleoceanographic changes in the Nordic Seas. Paleoceanography 18.
Rosqvist, G., Jonsson, C., Yam, R., Karlén, W., Shemesh, A., 2004. Diatom oxygen isotopes in pro-glacial lake sediments from northern Sweden: a 5000 year record of atmospheric circulation. Quat. Sci. Rev. 23, 851–859.
Rubensdotter, L., Rosqvist, G., 2009. Influence of geomorphological setting, fluvial-, glaciofluvial-and mass-movement processes on sedimentation in alpine lakes. The Holocene 19, 665–678.
Røthe, T.O., Bakke, J., Vasskog, K., Gjerde, M., D'Andrea, W.J., Bradley, R.S., 2015. Arctic Holocene glacier fluctuations reconstructed from lake sediments at Mitrahalvøya, Spitsbergen. Quat. Sci. Rev. 109, 111–125.
Sandgren, P., Snowball, I., 2001. Application of Mineral Magnetic Techniques to Paleolimnology, Tracking Environmental Change Using Lake Sediments. Springer, pp. 217–237.
Sejrup, H., Haflidason, H., Andrews, J., 2011. A Holocene North Atlantic SST record and regional climate variability. Quat. Sci. Rev. 30, 3181–3195.
Seppä, H., Birks, H.J.B., 2001. July mean temperature and annual precipitation trends during the Holocene in the Fennoscandian tree-line area: pollen-based climate reconstructions. The Holocene 11, 527–539.
Shakesby, R.A., Smith, J.G., Matthews, J.A., Winkler, S., Dresser, P.Q., Bakke, J., Dahl, S.O., Lie, Ø., Nesje, A., 2007. Reconstruction of Holocene glacier history from distal sources: glaciofluvial stream-bank mires and a glaciolacustrine sediment core near Sota Sæter, Breheimen, southern Norway. The Holocene 17, 729–745.
Sissons, J., 1979. Palaeoclimatic inferences from former glaciers in Scotland and the Lake district. Nature 278, 518–521.
Solomina, O.N., Bradley, R.S., Hodgson, D.A., Ivy-Ochs, S., Jomelli, V., Mackintosh, A.N., Nesje, A., Owen, L.A., Wanner, H., Wiles, G.C., 2015. Holocene glacier fluctuations. Quat. Sci. Rev. 111, 9–34.
Sutherland, D.G., 1984. Modern glacier characteristics as a basis for inferring former climates with particular reference to the Loch Lomond Stadial. Quat. Sci. Rev. 3, 291–309.
Syms, C., 2008. Principal components analysis. In: Jørgensen, S.E., Fath Brian, D. (Eds.), Encyclopedia of Ecology. Academic Press, Oxford, pp. 2940–2949.
Sønstegaard, E., Aa, A.R., Klakegg, O., 1999. Younger dryas glaciation in the Ålfoten area, western Norway; evidence from lake sediments and marginal moraines. Nor. Geol. Tidsskr. 79, 33–45.
Thomas, E.R., Wolff, E.W., Mulvaney, R., Steffensen, J.P., Johnsen, S.J., Arrowsmith, C., White, J.W., Vaughn, B., Popp, T., 2007. The 8.2 ka event from Greenland ice cores. Quat. Sci. Rev. 26, 70–81.
Trachsel, M., Nesje, A., 2015. Modelling annual mass balances of eight Scandinavian glaciers using statistical models. Cryosphere Discuss 9, 383–415.
Trouet, V., Esper, J., Graham, N.E., Baker, A., Scourse, J.D., Frank, D.C., 2009. Persistent positive North Atlantic oscillation mode dominated the medieval climate anomaly. Science 324, 78–80.
Trouet, V., Scourse, J., Raible, C., 2012. North Atlantic storminess and Atlantic meridional overturning circulation during the last millennium: reconciling contradictory proxy records of NAO variability. Glob. Planet. Change 84, 48–55.
Vasskog, K., Nesje, A., Støren, E.N., Waldmann, N., Chapron, E., Ariztegui, D., 2011. A Holocene record of snow-avalanche and flood activity reconstructed from a lacustrine sedimentary sequence in Oldevatnet, western Norway. The Holocene 21, 597–614.
Vasskog, K., Paasche, Ø., Nesje, A., Boyle, J.F., Birks, H.J.B., 2012. A new approach for reconstructing glacier variability based on lake sediments recording input from more than one glacier. Quat. Res. 77, 192–204.
Vinther, B.M., Clausen, H.B., Johnsen, S.J., Rasmussen, S.O., Andersen, K.K., Buchardt, S.L., Dahl-Jensen, D., Seierstad, I.K., Siggaard-Andersen, M.L., Steffensen, J.P., 2006. A synchronized dating of three Greenland ice cores throughout the Holocene. J. Geophys. Res. Atmos. (1984–2012) 111.
Wanner, H., Beer, J., Buetikofer, J., Crowley, T.J., Cubasch, U., Flueckiger, J., Goosse, H., Grosjean, M., Joos, F., Kaplan, J.O., 2008. Mid-to late Holocene climate change: an overview. Quat. Sci. Rev. 27, 1791–1828.
Wanner, H., Solomina, O., Grosjean, M., Ritz, S.P., Jetel, M., 2011. Structure and origin of Holocene cold events. Quat. Sci. Rev. 30, 3109–3123.
Wittmeier, H.E., Bakke, J., Vasskog, K., Trachsel, M., 2015. Reconstructing Holocene glacier activity at Langfjordjøkelen, Arctic Norway, using multi-proxy fingerprinting of distal glacier-fed lake sediments. Quat. Sci. Rev. 114, 78–99.